Bathymetry-constrained warm-mode melt estimates derived from analysing Oceanic Gateways in Antarctica

Lena Nicola[1,2], Ronja Reese[1,3], Moritz Kreuzer[1,2], Torsten Albrecht[1], and Ricarda Winkelmann[1,2]

[1] Potsdam Institute for Climate Impact Research (PIK), Member of the Leibniz Association, P.O. Box 60 12 03, D-14412 Potsdam, Germany

[2] Institute of Physics and Astronomy, University of Potsdam, Karl-Liebknecht-Str. 24-25, 14476 Potsdam, Germany

[3] Department of Geography and Environmental Sciences, Northumbria University, Ellison Place, NE1 8ST, Newcastle Upon Tyne, UK

Correspondence: Lena Nicola (lena.nicola@pik-potsdam.de) and Ricarda Winkelmann (ricarda.winkelmann@pik-potsdam.de)

Abstract. Melting underneath the floating ice shelves surrounding the Antarctic continent is a key process for the current and future mass loss of the Antarctic Ice Sheet. Troughs and sills on the continental shelf play a crucial role in modulating sub-shelf melt rates, as they can allow or block the access of relatively warm, modified Circumpolar Deep Water to ice-shelf cavities. Here we identify potential oceanic gateways in 7 out of 19 regions subdividing the Antarctic continent that could allow the access of warm water masses to Antarctic grounding lines, based on access depths inferred from high-resolution bathymetry data. We analyse the properties of water masses that are currently present in front of the ice shelf and that might intrude into the respective ice-shelf cavities in the future in case of changes in the ocean circulation. We use the ice-shelf cavity model PICO to estimate an upper bound of melt rate changes in case off-shore, intermediate layer warm water masses gain access to the cavities. We find that melt rates could increase in almost all regions at least by a factor of 1.5. Depending on the presence or absence of an oceanic gateway and the current ice-shelf melt conditions we find up to 42-fold larger basal melt rates. The identification of oceanic gateways is thus valuable for assessing the potential of ice-shelf cavities to switch from a 'cold' to a 'warm' state, which could result in widespread ice loss from Antarctica.

1 Introduction

The current mass loss from the Antarctic Ice Sheet is mainly triggered by thinning of the surrounding ice shelves (Pritchard et al., 2012; Paolo et al., 2015; Gudmundsson et al., 2019). This is caused by ice-shelf basal melting, that varies by orders of magnitude depending on the prevailing ocean conditions: a sub-shelf circulation that is initiated by sea-ice formation or tidal pumping and driven by the so-called 'ice pump' (mode 1 or 3-melting in Jacobs et al., 1992, respectively) causes melt rates at the order of centimetres to a few metres per year. For example, area-averaged observed melt rates at Filchner–Ronne Ice Shelf are around $0.3\pm0.1\ \mathrm{m\,yr^{-1}}$ (Ronne) and $0.4\pm0.1\ \mathrm{m\,yr^{-1}}$ (Filchner) as estimated by Rignot et al. (2013). In these ice shelves, mode 1 melting plays a major role towards the grounding line and mode 3 melting near the ice-shelf front (Silvano et al., 2016). Where melting is driven by Dense Shelf Water (mode 1) or surface waters (mode 3), generally water masses close to the surface freezing point are present within the cavity which can be hence classified as 'cold' – such as for Filchner–Ronne, Ross or Amery (Joughin et al., 2012; Silvano et al., 2016). Dense Shelf Water, due to the higher density from e.g. brine rejection from sea-ice formation, sinks to the ocean floor and spreads to the grounding line (Silvano et al., 2016). Ice-shelf thinning and upstream mass loss are currently not observed in these cold-cavity regions (Joughin et al., 2012; Paolo et al., 2015; Greene et al., 2022). A different mode of sub-shelf melting is driven by an inflow of water masses from the continental slope (mode 2-melting in Jacobs et al., 1992), bringing water with temperatures well above the pressure-melting point into the ice-shelf cavity. Such cavities can be classified as 'warm' (Joughin et al., 2012). They experience melt rates up to the order of tens of metres per year (cf. area-average basal melt rates for Pine Island and Thwaites in Rignot et al., 2013).

The exchange of water masses between the continental shelf and the open ocean is strongly influenced by bathymetry (Thoma et al., 2008; Nicholls et al., 2009; Hellmer et al., 2012; Pritchard et al., 2012; Tinto et al., 2019; Sun et al., 2022), but the processes that lead to on-shelf transport of warm water masses, leading to a switch to a 'warm' cavity and mode 2-melting, are highly complex and an active field of research. To what extent the inflow of warm waters from the continental-shelf break into ice-shelf cavities can be related to anthropogenic changes (Holland et al., 2022) or natural variability (Jenkins et al., 2016, 2018) alone, remains to be determined. Once, however, warmer water masses enter an ice-shelf cavity, this can lead to a strong increase in sub-shelf melt rates and in further consequence cause the adjacent ice streams to thin, accelerate, and retreat. Highest thinning rates in Antarctica are found for ice shelves in the Amundsen Sea, where relatively warm, modified Circumpolar Deep Water (mCDW) can access the ice shelves at depth through submarine troughs (Nitsche et al., 2007; Walker et al., 2007; De Rydt et al., 2014; Mouginot et al., 2014; Jenkins et al., 2016; Millan et al., 2017; Naughten et al., 2023). This mCDW comprises relatively warm and salty water masses which reside at mid-depth, on average at around 500 m, in the Southern Ocean in front of the continental shelf (Schmidtko et al., 2014; Holland et al., 2020).

Ocean access to ice-shelf cavities is generally modulated by geological structures on the continental shelf that block or channel the distal inflow of deeper and warmer water masses off the continental shelf, i.e. CDW. The abyssal Southern Ocean (here defined by a depth of <1800 m) raises towards the continent to form the shallow continental shelf that has a mean depth of about 500 m (Heywood et al., 2014), with the transition zone being called the continental-shelf break (CSB). The width of the continental shelf, which is the distance from the CSB to the coastline or ice sheet, varies around Antarctica from tens of kilometres, in East Antarctica or the West Antarctic Peninsula, to hundreds of kilometres in the Ross or Weddell Sea (Heywood et al., 2014). While large data gaps still exist, recent Antarctic bathymetry data incorporate major glacial troughs, ridges or other features of basal topography crosscutting the continental shelf (Arndt et al., 2013; Morlighem et al., 2020). These bathymetric features were mostly formed by erosion and sedimentation due to dynamic changes of the ice sheet during glacial cycles, e.g. ice streams leaving behind deep troughs when retreating (Bart, 2004; Hein et al., 2011; Morlighem et al., 2020).

The grounding line (or grounding zone, cf. Li et al., 2023), marks the transition between the grounded ice sheet and the floating ice shelves and thus constitutes the triple point of bedrock, ice, and ocean, see Fig. 1. Grounding lines in Antarctica can be found at depths down to 3000 m due to the erosion over long time scales. For individual ice shelves, sub-shelf melt rates are generally higher near the grounding line and lower towards the ice shelf's calving front (Lambert et al., 2023), if mode 3-melting is absent (Silvano et al., 2016). This general pattern is modulated by exchanges of water masses within the cavity and through other dynamical processes at play (e.g. the Coriolis effect). Ice-shelf thinning caused by melting close to the grounding line has been found to have the largest impact on the adjacent ice masses, resulting in higher fluxes across the grounding line due to a loss in buttressing (Reese et al., 2018b; Goldberg et al., 2019).

Distinct geological structures, such as troughs, are crucial boundary conditions for modelling ocean dynamics and the interaction of the ocean with the Antarctic Ice Sheet (Thoma et al., 2008; Hellmer et al., 2012), but previous studies do not systematically investigate the bathymetric access points or pathways to the grounding lines with regards to ice-sheet modelling and focus only on specific regions (see e.g. Herraiz-Borreguero et al., 2015; Tinto et al., 2019). Here, we present a simple approach to analyse *oceanic gateways* to the base of the Antarctic Ice Sheet, specifically to the ice-sheet's grounding lines. We identify oceanic gateways as the deepest topographic features that connect the deeper open ocean and the ice-shelf cavity, assuming that water follows this pathway, see Fig. 1. This assumption is motivated by Hellmer et al. (2012) and Naughten et al. (2021), that simulate an inflow of warm water masses through Filchner Trough which subsequently access large parts of the ice-shelf cavity. Our study provides a sensitivity-experiment, where in case of a trough-like feature, we assume the access of off-shore ocean water is possible (as in the case of Filchner Trough), leading to a drastic change in sub-shelf hydrography.

Where such a trough provide access to most of a region's grounding line, we identify this as ocean access via an oceanic gateway. The temperature of water masses found along such pathways, along the ice-shelf front, and towards the open ocean provides information about the water masses currently present within ice-shelf cavities. They also inform about the water masses that could potentially access the cavity through these pathways, if, for example, the Antarctic slope current near the continental-shelf break weakens and warm water masses can flow onto the continental shelf (Thompson et al., 2018). We combine observations of bedrock topography and ocean water masses to assess present-day pre-conditions for enhanced melting in all Antarctic regions. While no dynamic changes are taken into account, our analysis serves as a first-order assessment of an upper bound on melt rates that would be caused by an inflow of warm water masses at depth in Antarctica. Our approach of identifying relevant water masses that drive melting in cavities is also useful to improve the input for parameterisations of sub-shelf melt rates: for the ice-shelf cavity model PICO, for instance, temperature and salinity input are averaged over a certain depth to be used in the box model. With our analysis, we aim at better estimating this depth, by i.e. re-aligning the ocean regions over which input is averaged horizontally to include the relevant oceanic gateways.

On glacial time scales also the solid Earth response can shape the continental bathymetry and hence the ocean access to Antarctic grounding lines. In a related study, Kreuzer et al. (2023, in review) discuss potential changes in access depths and subsequent melt rates when considering relative sea-level changes resulting from deformational, gravitational, and rotational effects of the global redistribution of ice and ocean mass.

We describe our methodology in Sect. 2, followed by a presentation of the results in Sect. 3. In Sect. 4 we discuss our approach and findings, with a general conclusion included in Sect. 5.

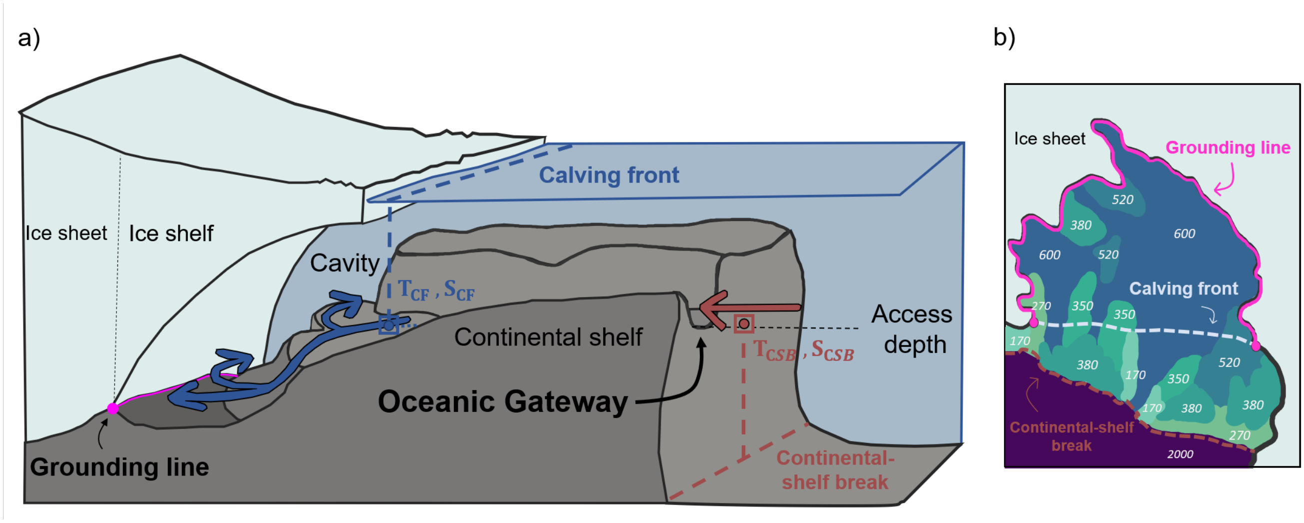

Figure 1. Illustration of used concepts in this study. a) Schematic of stylized oceanic gateway cross-cutting the continental shelf. Beyond the continental-shelf break, relatively warm Circumpolar Deep Water is present at mid depth. Its access to ice-shelf cavities is modulated by ocean circulation and bathymetry. Ocean temperatures at the bottom topography near the calving front (T_{CF}) provide information about the water masses that can already access the ice-shelf cavity (in the case of mode 1-melting, blue). If an oceanic gateway is present, water masses with a mean temperature T_{CSB} from the continental-shelf break (at the gateway's *access depth*, red arrow) can potentially reach large parts of the grounding line (triple point of bedrock, ice and ocean; magenta line) of the respective ice shelf. **b)** Access depths for each part of the continental shelf is obtained via a connected-component analysis. This yields a 2D field showing at what depths the ocean floor inside the ice-shelf cavity is connected to the open ocean. Analysing the 2D field at the grounding line of the region (magenta line) provides an estimate of the potential impacts when warm water masses are redirected from the continental-shelf break to the grounding lines.

2 Methodology

First we introduce the oceanic gateways concept (Sect. 2.1), then describe the used ocean data (Sect. 2.2) and summarise how we compute sub-shelf melting with PICO (Sect. 2.3).

2.1 Identifying oceanic gateways from bathymetry

Our analysis is based on BedMachine v3 bathymetry (Morlighem et al., 2020; Morlighem, 2022), which is provided on a 500×500 m grid spacing and contains ocean bathymetry from IBCSO v2 (Dorschel et al., 2022). From this, we calculate *access depths* for every location on the Antarctic continental shelf and in the ice-shelf cavities. The access depth, d, for each point on the continental shelf is the deepest vertical level (largest positive depth) in the open ocean for which there is a horizontal connection, not obstructed by bathymetry, to the water column above this point. We obtain these via a 'connected component analysis' (CCA). More specifically, we use the connected-component approach implemented by Khrulev (2024), with an algorithm similar to He et al. (2010). The algorithm iterates through the vertical column from 0 m to 3500 m spreads out in all horizontal directions, fills connected cells with the value of the depth at which they are connected, until it reaches boundaries or encounters obstacles i.e. cells with shallower bathymetry (the criterion is whether grid points are horizontally connected to the deep ocean at 3500 m or not). We have included Fig. S1 in the supplement to help visualising this analysis tool. As a result, our analysis yields circum-Antarctic access depths which are available as a 2D field on a 500 $\mathrm{m}\times$500 m horizontal grid spacing, following the resolution of the BedMachine data (Morlighem et al., 2020). When newer bathymetry fields become available, this data field can be easily updated with our processing scripts. We define the deepest access depth found along the grounding line of each basin as $\mathrm{d}_{\mathrm{GL},0}$ and express the fraction of how much the grounding line at that depth is connected to the open ocean with values ranging from 1 % to 100 %. If a large fraction of the grounding line is connected to the open ocean at the region's $\mathrm{d}_{\mathrm{GL},0}$, an oceanic gateway is present. An oceanic gateway can be seen as a horizontal pathway from the open ocean to the grounding line of the ice sheet along the deepest possible ocean-connection between the two. We here define the grounding line as the contour that delineates the contiguous grounded continental ice sheet (excluding larger islands and ice rises). We identify oceanic gateways for 19 Antarctic regions based on the drainage basins defined in Zwally et al. (2012) and extended into the ocean, with the Filchner–Ronne and Ross basins congregated as in Reese et al. (2018a).

2.2 Ocean properties

We analyse the properties of water masses based on the ISMIP6 ocean temperature and salinity climatology (Jourdain et al., 2020). The dataset is available at a 8 $\mathrm{km}\times$8 km horizontal and 60 m vertical resolution. The data points indicate temperatures and salinities averaged over the period 1995–2017. While observational datasets have many data gaps and thus do not provide sufficient horizontal as well as vertical coverage (especially on the continental shelf), the ISMIP6 fills these gaps with a specific extrapolation technique: while accounting for topographic barriers, the temperature and salinity fields from observations are extended, i.e., flooded into the ice-shelf cavities and regions below sea level that are currently covered by grounded ice. Due to this approach and the extended spatial coverage, we consider the ISMIP6 ocean dataset to be very well suited for our study. While the basic concept is the same, the ISMIP6 code is different to our analysis (Asay-Davis et al., 2020): our approach of quantifying the connectedness of the grounded ice to the open ocean aims at identifying pathways through which already existing warm water masses could fuel high melting rather than providing an extrapolated forcing field for projections. We therefore take into account the depth of grounding lines.

We extract ocean properties near the ice shelf's calving front, along the oceanic gateways as well as along the continental-shelf break, based on the local bathymetry and the access depths at the grounding lines for each basin $b = 1, 2, ...19$. The temperatures in front of the ice shelves (at the calving front) serve as a proxy for ocean water masses that can currently reach the ice shelves' deep grounding lines, similar to the case when mode 1-melting is dominant (cf. Silvano et al., 2016). The calving front (CF) is defined through the native BedMachine mask as the horizontal boundary between floating ice and the ocean. We calculate horizontal averages of temperature and salinity in the bottom layer, just above the bathymetry (topg), along the calving front and define $T_{\mathrm{CF,mean}}$ and $S_{\mathrm{CF,mean}}$ per basin as

$$T_{\text{CF, mean}}(b) = \text{mean}\,\{\,T(x,y,z)\,|\,(x,y)\in \text{CF}(b) \text{ and } z = \text{topg}(x,y)\} \tag{1}$$

and

$$S_{\text{CF, mean}}(b) = \text{mean}\{\, S(x,y,z) | \,(x,y) \in \text{CF}(b) \text{ and } z = \text{topg}(x,y)\}\,. \tag{2}$$

For estimating the change in melt rates, when assuming a basin-wide transition into a melt regime where melting becomes dominated by warm Circumpolar Deep Water (CDW) (mode 2 in Silvano et al., 2016), we derive properties along the continental-shelf break (CSB) at the deepest grounding line access depth for each basin and compare it to the estimates from the calving front, our proxies for mode 1-melting. We define the CSB to lie in an around 40 km-wide perimeter along the horizontal coordinates where the bathymetry is at a depth of 1800 m (i.e. a band of five grid cells along the 1800 m isobath). We assume that once warm water is flowing onto the continent, it will eventually reach the grounding line as CDW is not only warmer but also saltier and therefore denser than on-shelf waters. We thus expect it to sink from the shallowest overflow point eventually towards the grounding lines, filling up the cavity basin and replacing the less dense waters at lower depths.

We define the average temperature and sanility along this transect as $T_{\text{CSB, mean}}$ and $S_{\text{CSB, mean}}$, respectively, as

$$T_{\text{CSB, mean}}(b) = \text{mean}\{\, T(x,y,z) | \,(x,y) \in \text{CSB}(b) \text{ and } z = d_{\text{GL},0}(b)\} \tag{3}$$

and

$$S_{\text{CSB, mean}}(b) = \text{mean}\{\, S(x,y,z) | \,(x,y) \in \text{CSB}(b) \text{ and } z = d_{\text{GL},0}(b)\}\,. \tag{4}$$

Following different approaches to estimate an upper bound to melt rate changes, we will also use the maximum temperature found along the continental-shelf break to estimate melt rates, which we call $T_{\text{CSB, max}}$ and define as

$$T_{\text{CSB, max}}(b) = \max\{\, T(x,y,z) | \,(x,y) \in \text{CSB}(b) \text{ and } z = d_{\text{GL},0}(b)\}\,. \tag{5}$$

We will compare these estimates to the mean, but also the maximum temperatures found along the calving front $T_{\text{CF, max}}$,

$$T_{\text{CF, max}}(b) = \max\{\, T(x,y,z) | \,(x,y) \in \text{CF}(b) \text{ and } z = \text{topg}(x,y)\}\,. \tag{6}$$

To find the highest potential of temperature change, we therefore arrive at three ΔT-estimates:

$$\Delta T_{\text{mean-mean}}(b) = T_{\text{CSB, mean}}(b) - T_{\text{CF, mean}}(b), \tag{7}$$

$$\Delta T_{\text{max-mean}}(b) = T_{\text{CSB, max}}(b) - T_{\text{CF, mean}}(b), \tag{8}$$

and

$$\Delta T_{\text{max-max}}(b) = T_{\text{CSB, max}}(b) - T_{\text{CF, max}}(b). \tag{9}$$

The latter allows us to quantify the change in melting also in those regions, where melting is already driven by relatively warm water masses at depth i.e. where T_{CF} is already very warm.

2.3 Sub-shelf melting computed with the ice-shelf cavity model PICO

We compute the change in sub-shelf melt rates with the Potsdam Ice shelf cavity mOdel (PICO, Reese et al., 2018a). PICO extends the ocean box model by Olbers and Hellmer (2010) to be applicable in 3D-ice sheet models. It mimics the vertical overturning circulation present in ice-shelf cavities and can reproduce the wide range of average observed melt rates for 'warm' and 'cold' cavities. Ocean input is considered in PICO as an average per basin and once water masses reach the grounding line, they rise along the ice-shelf base towards the calving front, driven by the ice pump (Lewis and Perkin, 1986).

In Reese et al. (2023), PICO model parameters C (in $\mathrm{Sv\,m^3\,kg^{-1}}$) that describes the strength of the vertical overturning circulation and the heat-exchange coefficient γ_T^*, given in $10^{-5}\ \mathrm{m\,s^{-1}}$, are tuned to capture the sensitivity of melt rates to ocean temperature changes (cf. Reese et al., 2023). Input (T,S) to PICO in Reese et al. (2023) is based on temperature and salinity observations compiled by Schmidtko et al. (2014). In the tuning process, temperatures on the continental shelf were corrected for, similarly to the approach by Jourdain et al. (2020), such that the melt rates calculated by PICO match present-day observations compiled by Adusumilli et al. (2020). We here calculate melting resulting from a sudden warming of the cavities to the temperatures at the continental-shelf break by applying the differences $\Delta T_{\text{mean-mean}}$, $\Delta T_{\text{max-mean}}$, and $\Delta T_{\text{max-max}}$ as anomalies to the temperature fields from Reese et al. (2023).

To capture the parameter uncertainty in our estimates, we use the 'best' and 'max' parameter combinations from Reese et al. (2023); $\left\{C = 2.0\,\mathrm{Sv\,m^3\,kg^{-1}}, \gamma_T^* = 5\times10^{-5}\,\mathrm{m\,s^{-1}}\right\}$, and $\left\{C = 3.0\,\mathrm{Sv\,m^3\,kg^{-1}}, \gamma_T^* = 7\times10^{-5}\,\mathrm{m\,s^{-1}}\right\}$ respectively. The maximum number of boxes (N = 5) are used as in Reese et al. (2023). We use the PICO implementation in the Parallel Ice Sheet Model (PISM; https://www.pism.io; Bueler and Brown, 2009; Winkelmann et al., 2011) and as initial conditions ice thickness and bed topography from the BedMachine v3 dataset on a $4\ \mathrm{km}\times4\ \mathrm{km}$ grid spacing. We consider this resolution for estimating basal melt rates a good compromise between having a high resolution at the grounding line, on the one hand, and computational feasibility on the other hand.

3 Results

Our connected-component analysis yields a 2D field of access depths (see Supplement Fig. S2) that identifies which parts of the continental shelf are topographically connected to (i.e. on the same access depth) the individual ice-shelf regions. We use it to first update the existing basin boundaries by which the continental shelf is subdivided for in the PICO model. The boundaries on land are based on ice drainage basins from Zwally et al. (2012), were consolidated to 19 regions in Reese et al. (2018a) and for the use for PICO mainly extended along meridians into the ocean. In previous studies, those basin boundaries in the ocean were used to extract a basin average for temperature and salinity (i.e. average over the region) to feed into the box model. Figure 2 shows the new basin boundaries that we will use throughout this study. We have changed the basin boundaries near Filchner–Ronne and Amery ice shelves, inside the Amundsen Sea region and near George VI Ice Shelf in the Bellingshausen Sea based on the region's access depths. For this, we have extended their region's boundaries (by overlaying the access-depth field with the bathymetry) to incorporate the detected pathways through which warm water masses could gain access to the ice-shelf cavities. We have also aligned the basin boundary at the North tip of the Antarctic Peninsula with the local bathymetry

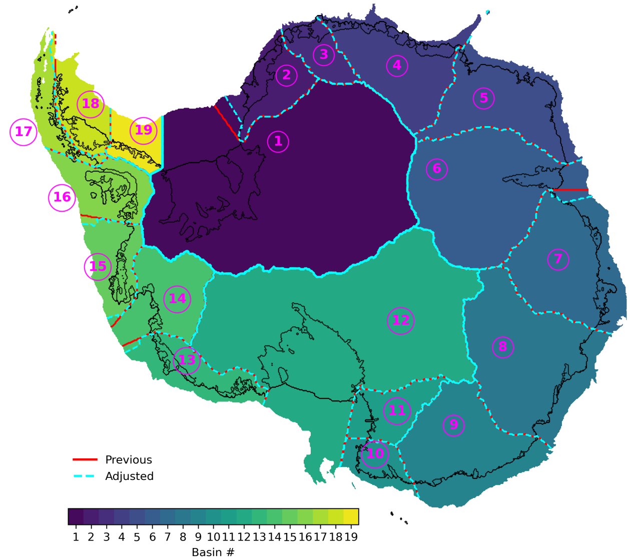

Figure 2. PICO model basin boundaries. The inland boundaries are based on satellite-derived drainage basins from Zwally et al. (2012) and were consolidated to 19 regions in Reese et al. (2018a). For the purpose of PICO, the basin boundaries were mostly extended along meridians into the ocean (red), which we have now partly adjusted (cyan) based on the derived access depths.

of the continental shelf. From here on forward, we use these updated basin boundaries and encourage other PICO users to do the same. We provide the new basin mask as NetCDF-file as well as the corresponding script to create those boundaries in our data repository. The 2D field of access depths for all locations on the Antarctic continental shelf and its ice-shelf cavities is provided in Supplement Fig. S2.

Figure 3 shows the main differences between the access-depth field and the bathymetry taken from BedMachine v3 Antarctica (Morlighem et al., 2020). This comparison highlights which parts of the continental shelf (and ice-shelf cavities) are shielded by topographic barriers, potentially blocking the access of warm water masses from the open ocean at depth. The most pronounced differences are found underneath Amery Ice Shelf, where the differences between the two fields can be larger than 1000 m. The deepest access depths evaluated at Antarctic grounding lines range from 283 to 610 m, with the deepest ocean access at Cook and Mertz Ice Shelves (basin 9) at 610 m, followed by 595 m at Filchner–Ronne (basin 1) to the shallowest of 283 m at the Western Antarctic Peninsula (basin 17). The latter region constitutes an exceptional case in our analysis, as its bathymetry is very shallow and it contains very few grounded areas. The distributions of the 2D access-depth field evaluated at a regions grounding lines are shown in Figure 4. The cumulative access to the region's grounding lines highlights those regions that are accessed by an oceanic gateway feature, i.e. a deep trough connecting the (overdeepened) ice-shelf cavity to the open ocean past the continental-shelf break, and thus accessing large portions of the grounding line at once. We find this feature in 7 out of 19 regions: Filchner–Ronne (basin 1), Amery (basin 6), Totten (basin 8), Rennick (basin 10), Drygalski (basin 11),

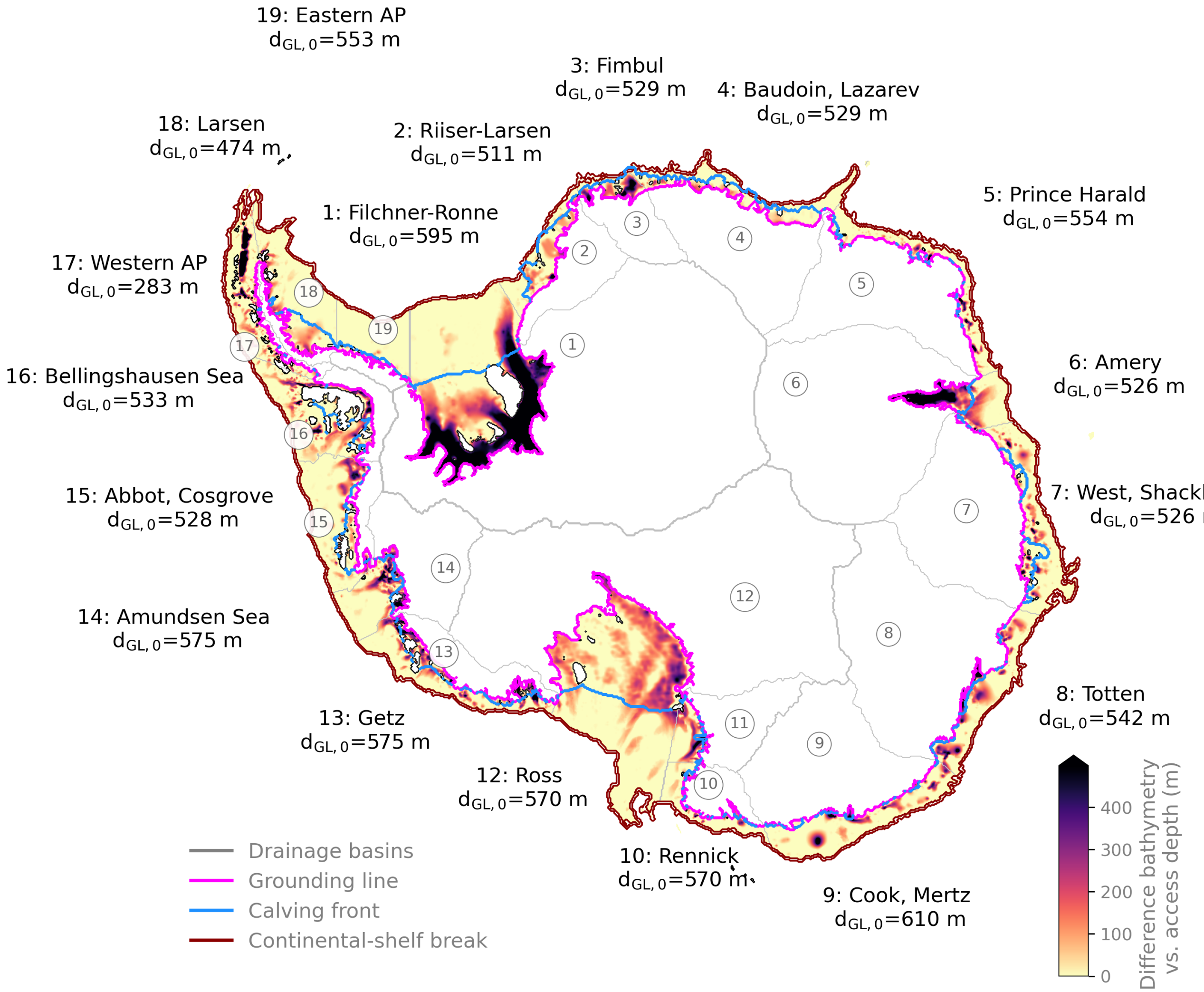

Figure 3. Regions of the Antarctic continental shelf shielded by topographic features. Color shading indicates the difference between the computed access depth over the continental shelf and in the ice-shelf cavities, compared to BedMachine v3 Antarctica bathymetry data (Morlighem et al., 2020). The drainage basins (grey outlines) are based on Zwally et al. (2012), consolidated as in Reese et al. (2018a), and labelled according to prominent ice shelves (with AP = Antarctic Peninsula). Coloured contour lines show the ice sheet's grounding line (magenta), the calving front (blue) and the continental-shelf break (red).

Ross (basin 12), and the Amundsen Sea region (basin 14). In Sect. 3.3, we will go into more detail which troughs constitutes those oceanic gateways. Supplement Fig. S3 shows the resulting access depths, when assigning the fraction of how much of the grounding line is connected to the open ocean to a specific depth (not vice versa, as shown in Fig. 4).

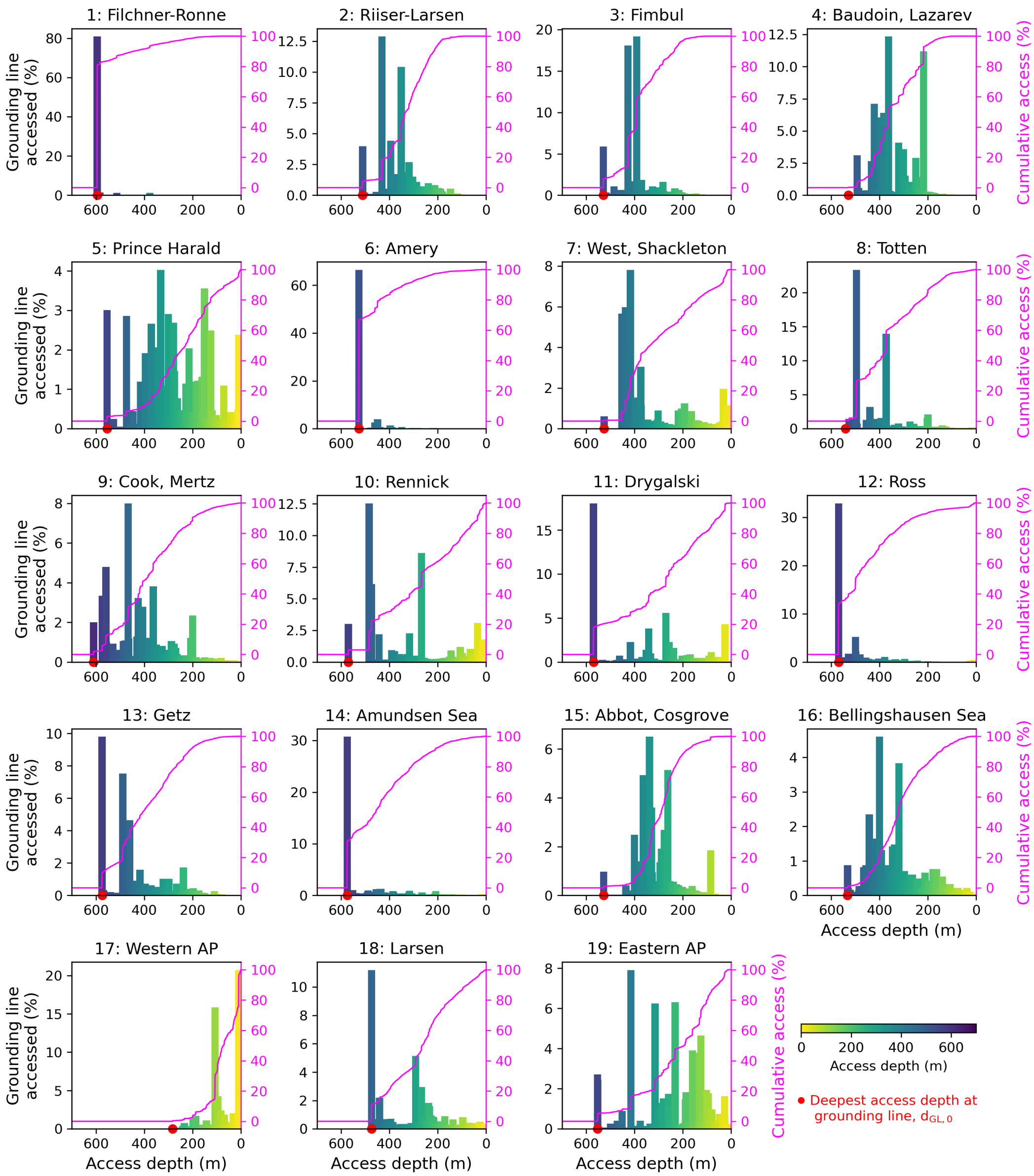

Figure 4. Distribution of access depths at region's grounding lines. For each depth level, it shows how much of the region's grounding line is accessed (fraction given in percent, bin width = 30). Magenta line shows the cumulative access, when adding up all depths levels. The drainage basins are based on Zwally et al. (2012), consolidated as in Reese et al. (2018a) and adjusted based on our access depth analysis (but only in the ocean, see above). The different regions are labelled according to prominent ice shelves (with AP = Antarctic Peninsula). Please note the different y-axis scales of the individual subplots.

3.1 Ocean properties extracted at access depths

Temperatures along the ice-shelf fronts, T_{CF}, which are evaluated at the ocean floor in the individual basins are in the mean much lower than temperatures found at the relevant access depth at the continental-shelf break, T_{CSB}, see Figure 5. This is not surprising as T_{CSB} incorporates the warm CDW which resides at mid-depth off the Antarctic continent, while T_{CF} oftentimes reflects the cold outflow of ice-shelf melt water at depth. Figure 5a shows the distribution of temperatures along these two locations for each basin. T_{CF} estimates range in the mean from -1.92°C at Filchner–Ronne to 0.19°C in basin 16 (Bellingshausen Sea). Especially in West Antarctica, the spread in T_{CF} is very large, compared to, for instance, the large ice-shelf regions of Filchner–Ronne, Ross or Amery. Mean temperatures along the continental-shelf break, $T_{\mathrm{CSB,mean}}$, range from -0.29°C in basin 2 (which incorporates the Riiser-Larsen Ice Shelf) to 1.74°C found in the Bellingshausen Sea region (basin 16). The maximum temperatures near the continental-shelf break, $\mathrm{T}_{\mathrm{CSB,max}}$ are highest in West Antarctica with the Bellingshausen Sea region reaching 1.86°C at maximum.

The temperature differences, shown in Figure 5b, range from 1.0 to 3.0°C when comparing mean estimates off-shore and along the calving front ($\Delta T_{\mathrm{mean-mean}}$), and from -0.2 to up to 2.96°C when comparing maximum temperatures ($\Delta T_{\mathrm{max,max}}$). We find the largest difference in basin 12 that incorporates Ross Ice Shelf ($\Delta T_{\mathrm{max-max}}$ = 2.96°C) and in basin 1 (Filchner–Ronne Ice Shelf) with $\Delta T_{\mathrm{max-max}}$ = 2.3°C. $T_{\mathrm{CF,max}}$>0°C are found in basins 2, 4, 5 and basins 8 to 10 in East Antarctica and in basins 13–18 i.e. in all West Antarctic basins (except Ross Ice Shelf), so that the difference to the continental-shelf break temperature is rather small. Especially in West Antarctica, high $T_{\mathrm{CF,max}}$ can be related to warm water already being present in some troughs along the calving fronts.

Since we want to provide an upper-bound estimate for bathymetry-constrained warm-mode melt rates, we employ the anomalies of $\Delta T_{\mathrm{max-mean}}$ (i.e. taking the highest continental-shelf break temperature and compare it to the basin-mean along the calving front). $\Delta T_{\mathrm{max-mean}}$ range from 1.6 to 3.3 °C, see Fig. 5b. It is interesting to note here, that for the big ice-shelf regions Filchner–Ronne, Ross and Amery, the way we obtain the temperature anomaly in case of basin-wide transition to warm mode melting does not matter much: $\Delta T_{\mathrm{mean-mean}}$, $\Delta T_{\mathrm{max-max}}$ and $\Delta T_{\mathrm{max-mean}}$ are very similar in these regions.

As the Drygalski region (basin 11) shares the continental-shelf break with the Ross region, we do not provide an estimate for T_{CSB} here. For this region, subsequent melt rates are not estimated either. Temperatures relative to the in situ freezing point, i.e. the thermal driving, is provided by in Supplement Fig. S5 and the actual PICO forcing temperatures are attached in Supplement Fig. S6.

In all basins, the water masses from the continental-shelf break are saltier than compared to those near the calving front ($S_{\mathrm{CSB}} > S_{\mathrm{CF}}$). The difference in the extracted salinity inputs is however small, ranging between nearly 0 PSU at Filchner–Ronne (basin 1) to 0.6 PSU at the Bellingshausen Sea region (basin 16). All salinity estimates are shown in Supplement Fig. S4.

3.2 Change in melt rates assuming basin wide transitions towards 'warm'-mode melting

Melt rates computed with PICO for the anomalous ocean temperatures and salinities are displayed in Figure 6. Almost all regions show a strong increase in sub-shelf melting when assuming that warm waters from the continental-shelf break can reach the ice-shelf cavities, all the way to the grounding line. Relative to their present-day estimates, melt rates increase most in the big ice-shelf regions of Amery, Filchner–Ronne and Ross that show a >20-fold increase in melting, cf. Fig. 6c, when assuming that warm waters from the continental-shelf break can access the respective ice-shelf cavities. Basal mass fluxes, using the 'max' PICO parameter combination as well as $\Delta T_{\text{max-mean}}$, mount to, for example, 3815 $\mathrm{Gt\,yr^{-1}}$ for Ross or 2367 $\mathrm{Gt\,yr^{-1}}$ for Filchner–Ronne Ice Shelf. We find the largest increase at Amery Ice Shelf, where melt rates could increase up to 42-fold, cf. Fig. 6c. Basin specific results will be further discussed and brought into line with the existing literature in the following. We assume that the increase in melting is mainly driven by the changes in temperature: the melting effect of the salinity differences of a maximum of 0.6 PSU, are by around one order of magnitude smaller.

In Section 3.3, we are looking more closely at the found oceanic gateways to major Antarctic ice shelves, while comparing the results from our analysis to existing observations and regional modelling studies.

3.3 Oceanic gateways to major Antarctic ice shelves

In the following, we are further analysing our results for the Filchner–Ronne Ice Shelf, Amery Ice Shelf, Ross Ice Shelf, ice shelves in the Amundsen Sea as well as in the Totten region in more detail.

3.3.1 Filchner–Ronne Ice Shelf

The Filchner–Ronne basin features an oceanic gateway at 595 m, through which around 75 % of the grounding line is horizontally connected to the open ocean. The identified oceanic gateway is Filchner Trough, which is a characteristic feature of the submarine topography in the Filchner–Ronne Ice Shelf region, see also Fig. 7. The trough extends from around Foundation Ice Stream to more than 450 km into the Southern Weddell Sea (distance measured from the ice-shelf front and taken from Larter et al., 2012). Its width varies between 125 to 175 km (Larter et al., 2012) and it terminates with a sill on its end towards the Weddell Sea (Hellmer et al., 2012). The sill depth determines the region's access depth in our study. As the mean depth of the basin's grounding lines is around 1000 m, water flowing in at the access depth of 595 m could reach much of the region's grounding zone at once. The deepest grounding lines are found down to around 2000 m in the BedMachine dataset (see Fig. 7 b).

At present, Filchner–Ronne Ice Shelf has a relatively cold cavity, with observed melt rates around $0.32 \pm 0.1\ \mathrm{m\,yr^{-1}}$ (Rignot et al., 2013). It currently contributes 10 % of the total ice-shelf mass loss around Antarctica (Mueller et al., 2018). In our analysis, water masses along the Filchner–Ronne calving front are close to the pressure melting point (with $T_{\mathrm{CF,mean}}$= -1.92°C at the ocean floor, cf. Fig. 7 c). A slope front in front of the ridge in Filchner Trough (Fig. 7 c) currently blocks warmer water masses that are present along the continental shelf (0.31°C in the mean or 0.53°C at maximum) from entering the cavity. If these were to enter the cavity, Filchner–Ronne would transition from a 'cold' to a 'warm' cavity, as also modelling studies suggest (Hellmer et al., 2012, 2017). At present, high-salinity shelf water (HSSW) is flowing into the ice-shelf cavity from the Ronne basin, while ice-shelf water (ISW) mainly flows outward through Filchner Trough (Nicholls et al., 2009; Naughten et al., 2021; Darelius et al., 2023). In our analysis, we also find colder HSSW residing in front of the sill of Filchner Trough on top of warmer water masses at depth, see Fig. 7 c. When assuming that warm water masses from the continental-shelf break reach all the way into the cavities, we estimate basal mass fluxes to be two orders of magnitude higher and increases from 73.8–78.1 $\mathrm{Gt\,yr^{-1}}$ in Reese et al. (2023), to 1466–1508 $\mathrm{Gt\,yr^{-1}}$ using average temperatures, depending on the used PICO parameter combination. Using the maximum temperatures along the two positions and the 'max' PICO parameter combination results in a basal mass flux of 2112 $\mathrm{Gt\,yr^{-1}}$. Melt rates increase from around 0.2 $\mathrm{m\,yr^{-1}}$ in Reese et al. (2023) to 3.8–5.5 $\mathrm{m\,yr^{-1}}$ which roughly correspond to the warm melt mode found at present near Getz Ice Shelf (cf. Reese et al., 2018a; Adusumilli et al., 2020). As the temperatures along the calving front do not have a wide spread, our derived temperature difference lie close together ($\Delta T_{\mathrm{mean-mean}}$= 2.2°C, $\Delta T_{\mathrm{max-max}}$=2.3°C and $\Delta T_{\mathrm{max-mean}}$=2.5°C). Our upper-bound estimate for Filchner–Ronne Ice Shelf using $\Delta T_{\mathrm{max-mean}}$= 2.5°C, yields a basal mass flux of 1685–2367 $\mathrm{m\,yr^{-1}}$ (depending on the PICO parameter combination).

Hellmer et al. (2012) found that a redirection of the slope current through Filchner Trough could occur within the 21st century under high greenhouse gas emissions and find a heightened basal mass flux of around 1600 $\mathrm{Gt\,yr^{-1}}$ on average. Naughten et al. (2021) find a two-timescale response of the Filchner–Ronne Ice Shelf under climate change, where warm water begins to intrude into the cavity only at approximately 7°C warming above pre-industrial levels. In an abrupt-4xCO2 scenario, due to the inflow of warm water masses, cavity temperatures are 2.7°C warmer, resulting in melt rates that are 21× higher than the control, > 1400 $\mathrm{Gt\,yr^{-1}}$. While our temperature differences of 2.2–2.5°C are slightly lower, our obtained basal melt estimates are very close to the published literature. As for the drivers for such a regime shift, Haid et al. (2022) find that the density balance between the shelf waters originating from sea-ice production and the warmer water at the continental-shelf break as the most decisive factor for the Filchner–Ronne ice-shelf cavity to tip into a warm state.

3.3.2 Amery Ice Shelf

Towards Amery Ice Shelf, we identify a gateway through Prydz Channel, see Fig. 8, along which the Amery grounding zone has retreated since the Last Glacial Maximum (Mackintosh et al., 2014). Prydz Channel is thus another example that shows that gateway-like features can oftentimes be linked to glacial erosion. The grounding line of Amery Ice Shelf lies very deep, at a mean depth of around 1100 m in the BedMachine dataset, while the deepest parts of the grounding line are found at 2950 m depth (see Fig. 8 b). Once water flows onto the continental shelf at a depth of $\mathrm{d_{GL,0}}$ = 525 m, it could potentially reach large parts of the basin's grounding line (>60 % in our analysis).

The temperatures at the ocean floor near the calving front are -1.84°C on average. At the continental-shelf break, the mean temperature is 0.35°C, but temperatures are up to 0.60°C at maximum. When it comes to average melt rates, Rignot et al. (2013) list observed melt rates at Amery Ice Shelf as 0.6±0.4 $\mathrm{m\,yr^{-1}}$. In our study, melt rates would increase to 12.4–21.43 $\mathrm{m\,yr^{-1}}$ (depending on the PICO parameter combination), when applying the temperature anomaly of 2.2°C ($\Delta T_{\text{mean-mean}}$) and 1.9°C ($\Delta T_{\text{max-max}}$).

Our upper-bound estimate for Amery Ice Shelf using $\Delta T_{\mathrm{max-mean}}$= 2.4°C, yields a basal mass flux of 958–1339 $\mathrm{m\,yr^{-1}}$ (depending on the PICO parameter combination).

If warm CDW residing at the continental-shelf break will actually pass through the identified gateway remains uncertain. Williams et al. (2016) find a different pathway of modified Circumpolar Deep Water towards Amery Ice Shelf, through Four Ladies Bank more to the East, see Fig. 8 a, which is much shallower than Prydz Channel. Here our core assumption that CDW always takes the deepest entry / gateway towards the ice shelf is challenged. Our quantitative estimates however fit to a recent preprint, in which Jin et al. (2024), using a regional ocean model, show that melt rates could reach up to 17 $\mathrm{m\,yr^{-1}}$ given a regime shift in the next century under a high-emission scenario. Amery Ice Shelf is located downstream of Lambert glacier that is draining about 16 % of the grounded East Antarctic Ice Sheet (Fricker et al., 2000). Enhanced melting due to warm water inflow at depth could hence produce an increase in sea-level contribution from large portions of the East Antarctic Ice Sheet.

3.3.3 Ross Ice Shelf

For the majority of the Ross Ice Shelf cavity, we identify the Glomar Challenger Basin (see also Fig. 9) as the topographic feature which provides access at the depth of 570 m. The basin is a north-east trending cross-shelf paleo-trough (Owolana, 2011). We determine its lower lying western sub-basin as an important gateway, that provides access to around 30 % of the basin's grounding line. At 570 m, the grounding lines of Mac Ayeal, Bindschadler and Mercer/Willans Ice Streams (Western side) are reached as well as the grounding line of Byrd Glacier on the eastern side of Ross Ice Shelf. The mean depth of the basin's grounding lines is rather shallow at around 575 m, but can reach around 1000 m in the BedMachine dataset (see Fig. 9 b). These deep-lying grounding lines are accessed at the critical depth of 570 m.

Similar to FRIS, cold water masses are found along the ice-shelf front (Fig. 9 c) with warmer water masses beyond the continental slope front). The derived temperatures are at -1.89°C near the calving front and 1.12°C in the mean at the continental-shelf break, with temperatures of up to $T_{\mathrm{CSB,max}}$= 1.38°C.

Observed melt rates lie at 0.0±0.1 $\mathrm{m\,yr^{-1}}$ for the Western and 0.3±0.1 $\mathrm{m\,yr^{-1}}$ for the eastern part of the ice shelf (Rignot et al., 2013). The Ross basin can hence be classified as a 'cold' cavity, like Filchner–Ronne Ice Shelf. Present-day melt rates from Reese et al. (2023) lie at 0.3 $\mathrm{m\,yr^{-1}}$. Melt rates increase to 5.4–7.8 $\mathrm{m\,yr^{-1}}$ assuming a transition to mode 2-melting by 3.0°C warmer water entering the cavity ($\Delta T_{\mathrm{mean-mean}}$=3.3°C). This corresponds to a roughly 24-fold increase in basal mass flux from around 130 $\mathrm{Gt\,yr^{-1}}$ to 2357–3372 $\mathrm{Gt\,yr^{-1}}$. Our bathymetry-constrained upper-bound estimate for Ross Ice Shelf using $\Delta T_{\mathrm{max-mean}}$=3.3°C, yields a basal mass flux of 2777–3815 $\mathrm{m\,yr^{-1}}$ (depending on the PICO parameter combination).

Tinto et al. (2019) find that high-salinity shelf water flows under the ice front near Ross Island to the East, then moves southward towards the East Antarctic side of the ice shelf, and eventually exits through Glomar Challenger Trough to the Ross Sea. They highlight that the tectonic boundary between the East and West Antarctic side of Ross Ice Shelf impact the vulnerability to sub-shelf melting, since the part of the cavity near Siple Coast is rather isolated from the influence of in-flowing (warm) water masses. Here we assume, however, an inflow of warm water masses through Glomar Challenger Basin reaching those ice streams, given an access of water masses at the critical depth of 570 m. Nonetheless, the rest of the cavity near

Siple Coast shows generally more shallow access depths in our analysis, which can be linked to the tectonic boundary and the difference in the crustal composition that influence the bathymetry (Tinto et al., 2019).

At a depth of 570 m, we find that 15 % of the grounding line near Drygalski Ice Tongue (basin 11) is connected to the open ocean as well, which is linked to the access depth underneath Ross Ice Shelf.

3.3.4 Ice shelves in the Amundsen Sea

In the Amundsen Sea region, the most direct connection to the open ocean is Abbot Cosgrove Trough, a 760 m deep feature that evolved through erosion along a paleo ice stream across the continental shelf (Hochmuth and Gohl, 2013; Klages et al., 2015). Abbot Cosgrove Trough feeds into Pine-Island Thwaites Trough, close to the 'Eastern Trough' as often referred to in the literature (see e.g. Dutrieux et al., 2014). However, the deepest access depth found at the grounding line in this basin is dominated by the access through Dotson-Getz Trough (at 575 m), that enables a pathway for water masses from Getz Ice Shelf (accessed via the Western Getz / Siple Trough from the open ocean, see Fig. 10) through Dotson and Crosson Ice Shelves eventually reaching Thwaites and Pine Island. These results need to be taken with caution, as under ice-shelf bathymetry are associated with high uncertainty.

The mean depth of this basin's grounding line is at around 680 m, but the deepest parts lie at < 1500 m, that are reached by the access depth, $\mathrm{d}_{\mathrm{GL},0}$. Warm water masses are present along the entire transect from the deep ocean up to the ice-shelf front (Fig. 10 c).

We derive a mean temperature of $T_{\mathrm{CF,mean}}$=-0.23°C near the calving fronts of this region. This is considerably cooler than the near-bottom temperature presented in Dutrieux et al. (2014), namely 1.2°C in 2012 at the Pine Island Glacier calving front. This average is much closer to our T_{CSB} estimates for that region, $T_{\mathrm{CSB,mean}}$ = 1.42 °C and $T_{\mathrm{CSB,max}}$ = 1.54 °C. However, in Fig. 5, we have shown the large spread in temperatures along the calving front in this basin. The highest temperatures along the calving front are found near Pine Island Glacier with a maximum temperature of $T_{\mathrm{CF,max}}$=1.17 °C. With this, the difference to $T_{\mathrm{CSB,max}}$ is only 0.4 °C.

Pine Island Glacier with observed melt rates of 16.2±1.0 $\mathrm{m\,yr^{-1}}$ and Thwaites glacier with 17.73±1.90 $\mathrm{m\,yr^{-1}}$, respectively, have been considered belonging to one basin in our analysis: The melting could increase to 19.9–48.45 $\mathrm{m\,yr^{-1}}$ when assuming that (more) warm water from the continental-shelf break can access the grounding lines of this basin. Applying the difference in mean temperatures, $\Delta T_{\mathrm{mean-mean}}$=1.6 °C, corresponds to a 2.7–3.4-fold increase in basal mass flux, from 208.9–209.9 $\mathrm{Gt\,yr^{-1}}$ in Reese et al. (2023) to 569–703 $\mathrm{Gt\,yr^{-1}}$ (depending on the PICO parameter combination) in our analysis. Using the difference in maximum temperatures and the 'max' parameter combination is, however, only 314 $\mathrm{Gt\,yr^{-1}}$ (1.5–fold increase) corresponding to the small temperature difference of 0.4°C. In our study, this change is the second lowest, with Getz Ice Shelf (basin 13) experience almost no change in melting, with $\Delta T_{\mathrm{max-max}}$=0.001°C. Using mean temperatures, basin 13 could however see a temperature increase of $\Delta T_{\mathrm{max-max}}$=2.23°C. Our bathymetry-constrained upper-bound estimate for the Amundsen basin using $\Delta T_{\mathrm{max-mean}}$=1.8°C, yields a basal mass flux of 598–742 $\mathrm{m\,yr^{-1}}$ (depending on the PICO parameter combination).

At present, ice shelves in the Amundsen Sea have 'warm' cavities and therefore dominate the current mass loss in Antarctica (see e.g. Pritchard et al., 2012), indicating that this region is already out of balance with the current oceanic forcing.

How else do our findings fit to the published literature? Thoma et al. (2008) simulate an inflow of CDW onto the Amundsen shelf and find that the warm water reaching Pine Island Bay are guided trough a submarine trough reaching to the continental-shelf break, close to where we estimate the continental-shelf break temperatures T_{CSB} in our study. Haigh et al. (2023) find that the ridge that is indicated in our study as the overflow point (see Fig. 10 c), blocks inflow from the Bellingshausen Sea at depth, so that water masses rather originate from the Pine Island Thwaites Trough, similar to Thoma et al. (2008) and Naughten et al. (2022). Gómez-Valdivia et al. (2023) employ a global climate model on a relatively coarse resolution (1° ocean model) and find a shift in currents in the Amundsen Sea sector, leading to an enhanced onshore transport of CDW and an increase in ocean temperatures by 1.2°C. Our estimate in melt rate increase is thus an upper-bound estimate, as 2.23°C is the largest difference we can obtain with our algorithm (cf. Fig. 5).

3.3.5 Ice shelves in the Totten region

The Totten region that incorporates Totten and Moscow University Ice Shelf has a direct ocean access to 25 % of their total grounding lines at an access depth of 496 m through a trough near the Law Dome peninsula, see Fig. 11. $\mathrm{d}_{\mathrm{GL},0}$ is 542 m however, meaning that there are some deeper grounding line parts that have a deeper horizontal connection to the ocean, see the Totten sub-panel in Fig. 4. The mean depth of the basin's grounding line is 635 m, but the deepest parts go down to <2500 m. Our analysis shows that those deep parts of the grounding line at Totten Ice Shelf are connected to the open ocean at a depth of 496 m. Moscow University Ice Shelf has a slightly shallower access depth of 384 m (see the second spike Fig. 4), compared to Totten Ice Shelf. In the ISMIP6 climatology, warm temperatures are not only present along the continental-shelf break but can also be found on the continental shelf in front of Totten Glacier (cf. Fig. 11, c).

Rignot et al. (2013) find melt rates at Totten Ice Shelf to be 10.47±0.7 $\mathrm{m\,yr^{-1}}$. According to our analysis, melt rates at Totten would see an around 3.3–4.1-fold increase in basal mass flux, from around 90 $\mathrm{Gt\,yr^{-1}}$ to 289–367 $\mathrm{Gt\,yr^{-1}}$ (around 7 to 23.1–29.4 $\mathrm{m\,yr^{-1}}$) when assuming an inflow from the warmest waters near the continental-shelf break at 496 m. Those water masses are 1.2°C warmer compared to those present at the ocean floor near the calving front. The mean temperatures differ by 2.1°C. Totten Ice Shelf is the floating extension of Totten Glacier, that drains a catchment containing ice with an equivalent of 3.5 m of global sea-level potential (Greenbaum et al., 2015), and currently experiences the largest thinning rate of all East Antarctic regions (Pritchard et al., 2009; Flament and Rémy, 2012; Greenbaum et al., 2015). Here, elevated sub-shelf melt rates due to warm water inflow onto the continental shelf could already be the cause for the adjacent glacier to thin. Further ocean-induced melting can therefore have significant consequences to global sea-level rise. Moscow University Ice Shelf is included in the same region as Totten Ice Shelf. From our analysis, we determine the relevant access depth, $\mathrm{d}_{\mathrm{GL},0}$ to be 373 m, which resembles the second spike in the distribution when evaluating the access depths of the entire region's grounding line(s), see Fig. 4. For more specific regional results, the two ice shelves need to be treated as separate basins.

3.4 Other regions

The deepest access depth found at the grounding zone around Fimbul Ice Shelf within basin 3 is 529 m, which only encompasses 5 % of the total region's grounding line. The basin incorporates several ice shelves, including Jelbart and Ekström Ice Shelf. When plotting how much of the grounding line can be accessed at which depth (Fig. S3), we determine ocean access through two gateway structures: the grounding line of Jelbart Ice Shelf is connected to the open ocean at 427 m and the grounding zone of Ekström Ice Shelf in the same region is connected at a depth of 391 m, indicating that ocean access to the different ice-shelf cavities is achieved by individual troughs connected the ice-shelves to the open ocean. More information on the sub-shelf bathymetry in this region is given in Eisermann et al. (2020). Our findings for basin 3 here stand as another example that the PICO basin boundaries need to be further refined to obtain more specific regional results.

4 Discussion

Our data analysis infers potential pathways for warm water inflow into ice-shelf cavities from access depths for 19 drainage basins in Antarctica and provides estimates for changes in sub-shelf melt rates.

The results of the analysis need to be evaluated in light of the key assumptions and limitations of our approach: firstly, we assume that ocean waters in front of the ice shelf serve as valid proxy for water masses that currently drive melting underneath the ice shelf, which is generally valid for cold-mode ice shelves, but not for shelves with warm-mode melting (Silvano et al., 2016). Not all ice shelves are considered cold-mode ice shelves at present, most notably the ice shelves in the Amundsen Sea region. Second, we estimate the continental-shelf break temperatures at the region's deepest grounding line access depth, $\mathrm{d}_{\mathrm{GL},0}$, assuming that water masses simply follow the bathymetry when flowing onto the shelf, and not follow isopycnals (Drijfhout et al., 2013). Ocean dynamics, which crucially determine sub-shelf circulation patterns and thereby influence the access potential (Nicholls et al., 2009; Williams et al., 2016), are not considered in this study. Our analysis is thus a sole representation of the role of the geometry of the continental shelf including the ice-shelf cavities and connecting features such as the oceanic gateways. Our study could therefore be improved by considering specific ocean circulation patterns informed by high-resolution ocean models, such as in Naughten et al. (2023), that can also assess the boundary conditions for mode 2 onset in all regions.

Cold and dense shelf waters flowing out of ice-shelf cavities generally shield the ice shelf from warm CDW inflow at depth (Janout et al., 2021). The circulation patterns in the ice-shelf cavity system such as Filchner–Ronne, are strongly controlled by dynamical processes, for instance by the Coriolis force or, for instance, the interplay of sea-ice production and polynya formation which is in turn linked to anomalies in the large-scale atmospheric circulation around Antarctica (Alley et al., 2015; Janout et al., 2021; Haid et al., 2022). However, our identified gateways could be an entry point to cross-cut the density barrier (i.e. the Antarctic Slope Current) in front of the continental shelf (Hirano et al., 2023). Furthermore, changes in the thermocline depth and resulting changes in density could lift up water masses over topographic features (Assmann et al., 2013; Dutrieux et al., 2014; Hattermann, 2018; Daae et al., 2020). Here again, high-resolution ocean dynamical models could suggest that access is more likely through shallower channels, or that even deeper ocean levels than at access depth should be considered.

Typically, if CDW flows onto the continental shelf, it mixes with fresh and colder on-shelf water masses (Wang et al., 2023). This modified Circumpolar Deep Water (mCDW) is generally colder than the temperatures estimated in this study: Williams et al. (2016) define the maximum potential temperature of mCDW to lie between -1.7 and 0°C, while Ribeiro et al. (2021) use a range from -1.7 to 1.5°C for mCDW, when classifying water masses near Totten Ice Shelf. Only the mean temperatures at the continental-shelf break for basins 15 and 16 would lie above this range. Since we neglect the modification of Circumpolar Deep Water when accessing the grounding lines in the ice-shelf cavities, our findings should be understood as upper-bound estimates.

In addition to these overarching structural limitations, additional uncertainties arise from the methodology and data: our analysis algorithm is based on the bathymetric structures and characteristics which are represented in the BedMachine data. We apply our algorithm on the dataset grid resolution (at a $500\ \mathrm{m}\times500\ \mathrm{m}$ grid spacing) which we think is crucial to preserve features that are resolved at that scale. Even higher resolutions would allow a more precise analysis of the topographic structures, but this would require higher computational resources, and main features of the present-day bathymetry might be well-resolved at the current grid spacing already. A resolution of $500\ \mathrm{m}$ in the BedMachine Dataset is the current state-of-the-art and incorporates most recent findings. As the oceanic gateways may require a certain width for the dynamic inflow of ocean water, even higher resolutions may not provide more reasonable insights. We here assume that a minimum channel width of $500\ \mathrm{m}$ as resolved by the dataset, is wide enough to fill the trough and subsequent cavity with off-shore warm water during a sustained inflow.

We further assume that the bathymetry is time-invariant, which is not the case when considering longer time scales. Sill depths and grounding line location and thus access depths may change by hundreds of meters in response to erosion, sea-level changes and glacial isostatic adjustment effects (see Kreuzer et al., 2023, in review).

Cavity-resolving ocean models are computational very expensive and therefore limited to simulations on centennial timescales. Large-scale modelling studies thus often rely on parameterisations to infer ocean-driven sub-shelf melting. We here use the PICO model to estimate sub-shelf melt rates based on the temperatures and salinities in front of the ice shelves as well as from the continental shelf-break. Favier et al. (2019) find that a box parameterisation that mimics the vertical overturning in the cavity, such as PICO, provides melt estimates that are comparable to coupled ice-ocean simulations. However, our melt rate estimates could differ when using an alternative melt parameterisation or assuming a higher melt rate sensitivity to thermal forcing, e.g. by using a quadratic melt relationship (Burgard et al., 2022). It is to note here that Burgard et al. (2022) does not find good agreement between PICO and a reference coupled model, but the PICO implementation in that study also uses a completely different PICO parameter tuning. In our study, we assume that once waters can reach the grounding line it can access all parts, as one temperature and salinity estimate is applied to the whole length of the grounding line in the box model. With a spatially more resolved approach, one could apply the extracted temperature forcing to only those parts of the grounding lines that are connected to the open ocean at the deepest access depth found at the ice-shelf region's grounding line.

PICO does not include horizontal ocean circulation, modification of water masses on the continental shelf or blocking of water masses entering the continental shelf nor mode 3-melting (where surface waters cause melting near the ice-shelf front). This might bias melt rates in cold cavities at the moment. Furthermore, the melt pattern in PICO is less resolved, melt rates are more distributed than in ocean circulation models, and PICO does not reach the very high melting found close to grounding lines (Dutrieux et al., 2014; Paolo et al., 2015). The relevance of this for ice sheet model studies needs to be further assessed (some first analyses were done in Reese et al., 2018b). A recent study suggested that bulk melting is more relevant than spatial patterns for the small, constrained Pine Island Glacier Ice Shelf (Joughin et al., 2021). The question if bulk melting or the melt pattern is more relevant, is not resolved yet, but our study does not aim to estimate this and we would hence refer to future work.

Furthermore, we use only two parameter combinations for the overturning and heat exchange coefficients in PISM-PICO, to capture to some extent the parameter uncertainty in the melt estimates when assuming a warm water inflow from the continental-shelf break. We use those parameter sets that were selected to match the sensitivity of melt rates to temperature changes for present-day Antarctica (Reese et al., 2023). However, a full model ensemble would be required to estimate the full uncertainty that arises from the choice of the PICO parameters. Despite these limitations, we want to stress that melt parameterisations such as PICO are essential for large-ensemble studies or long-term studies that cavity-resolving ocean circulation models cannot cover due to computational costs; they will thus serve an important purpose also in future ice-sheet model simulations and projections.

As we have shown, the analysis of access depths on the continental shelf helps to better inform the basin boundaries in PICO, that could be applied to different melt parameterisation in ice-sheet models as well. However, there are a number of alternative subdivisions of the Antarctic continent, as for example in van der Linden et al. (2023), in which they differentiate between the Ross, Amundsen, Weddell, Peninsula, and an East Antarctic Ice Sheet ocean sector. In the Ross Sea however, they separate between the ocean in front of Victoria land (Drygalski region) and the rest of the Ross Sea. This makes their classification not suitable for our analysis, as we consider the continental-shelf break in front of Ross Sea representative for both regions.

When it comes to the effects of the potential warm water inflow as analysed in our study, the difference in temperatures is small in some regions for physical reasons: this can be the case if the access depth of the basin is shallow and encompasses slightly colder water masses at the CSB, or if the calving front temperatures are already relatively warm, as in the case of the Amundsen region. In those regions, the difference in temperatures is higher when comparing mean conditions.

The temporal evolution of warm water accessing the Antarctic grounding lines at depth depends on the complex interplay of ice, ocean, atmosphere, and solid Earth. Importantly, the timing would mainly depend on the future climate change scenario determining the change in oceanic boundary conditions. We here aim at quantifying the potential effect this might have in the future. Ocean model projections show that warm water access under the Filchner–Ronne Ice Shelf may occur due to ongoing climate change, but that it is unlikely to happen within the next decades (Hellmer et al., 2012; Naughten et al., 2021; Haid et al., 2022). Other regions might also be susceptible to a basin-scale transition to mode 2-melting: When assuming that sub-shelf melting becomes intensified by warm water from the continental-shelf break, Jordan et al. (2023) find that the East Antarctic Ice Sheet might lose up to 48 mm of sea-level equivalent ice volume over the next 200 years. However, they artificially alter the ocean forcing to represent a shift to stronger on-shelf CDW transport. All in all, cavity geometries are highly heterogeneous and the impact of the onset of mode 2-melting should thus be determined individually in a follow-up study taking into account other measures for the response of the grounding line, e.g. buttressing, as in Naughten et al. (2023). Our analysis follows only an idealized approach; for realistic projections of potential future regime shifts in the Antarctic ice-shelf regions, more sophisticated approaches are needed. These approaches at best have a coupled ice-ocean-atmosphere representation, with interactive ice sheets and ice shelves at high resolution in space and time.

5 Conclusion

In our study, we present a simple approach to calculate the access depths of water masses to Antarctic grounding lines. We combine latest available bathymetry data with present-day ocean temperature and salinity data. Thereby, we identify oceanic gateways in 7 out of 19 regions through which warm water masses residing off the continental-shelf break could potentially access large parts of the deep grounding lines in several Antarctic regions. Warm-water inflow to regions with deep-lying grounding lines and subsequent increased sub-shelf melting can have a strong impact on the ice flux across the grounding line and therefore the overall mass balance of the Antarctic Ice Sheet (Reese et al., 2018b; Goldberg et al., 2019).

Perturbing the current state of the Antarctic Ice Sheet with warmer temperatures at the continental-shelf break helps estimating an upper bound on melt rate changes. All regions would experience a strong increase in sub-shelf melting, while basal melt rates would shift by up to two orders of magnitudes in cavities that are currently in a 'cold' state. We estimate an increase in temperatures at a maximum of 3.3°C. As our quantitative results match findings from regional modelling studies that exist in some basins, we are cautiously optimistic that our findings can be taken as upper-bound estimates for other regions too. The increase in temperature we estimate here could hence be employed by ice-sheet modellers to calculate an upper-bound estimate of the consequences of a flip of all Antarctic cavities into a warm state for current ocean conditions.

While high-resolution ocean modelling could provide a more detailed estimate on the effect of oceanic gateways on melting, our first-order approach is instead straight-forward and easy to run, meaning that only a few analysis scripts are necessary to (re-)produce our results. When new bathymetry or ocean temperature data becomes available, our study can be repeated in an instant, even on a $500\ \mathrm{m} \times 500\ \mathrm{m}$ grid spacing (within < 10 minutes). The presented approach serves as a refinement on identifying those ocean regions most relevant as input for PICO or other melt parameterisation. As mentioned above, we recommend other PICO users to take into account the connectedness of the continental bathymetry when preparing the relevant input data.

To conclude, by identifying potential ocean gateways and analysing the thermal properties of ambient water masses, our study contributes to assessing the current and potential future vulnerability of the Antarctic Ice Sheet to changes in its surrounding ocean.

Code and data availability. The data and relevant code will be made publicly available on a public data repository i.e. PANGAEA or Zenodo. DOI links to the repositories will be provided upon publication.

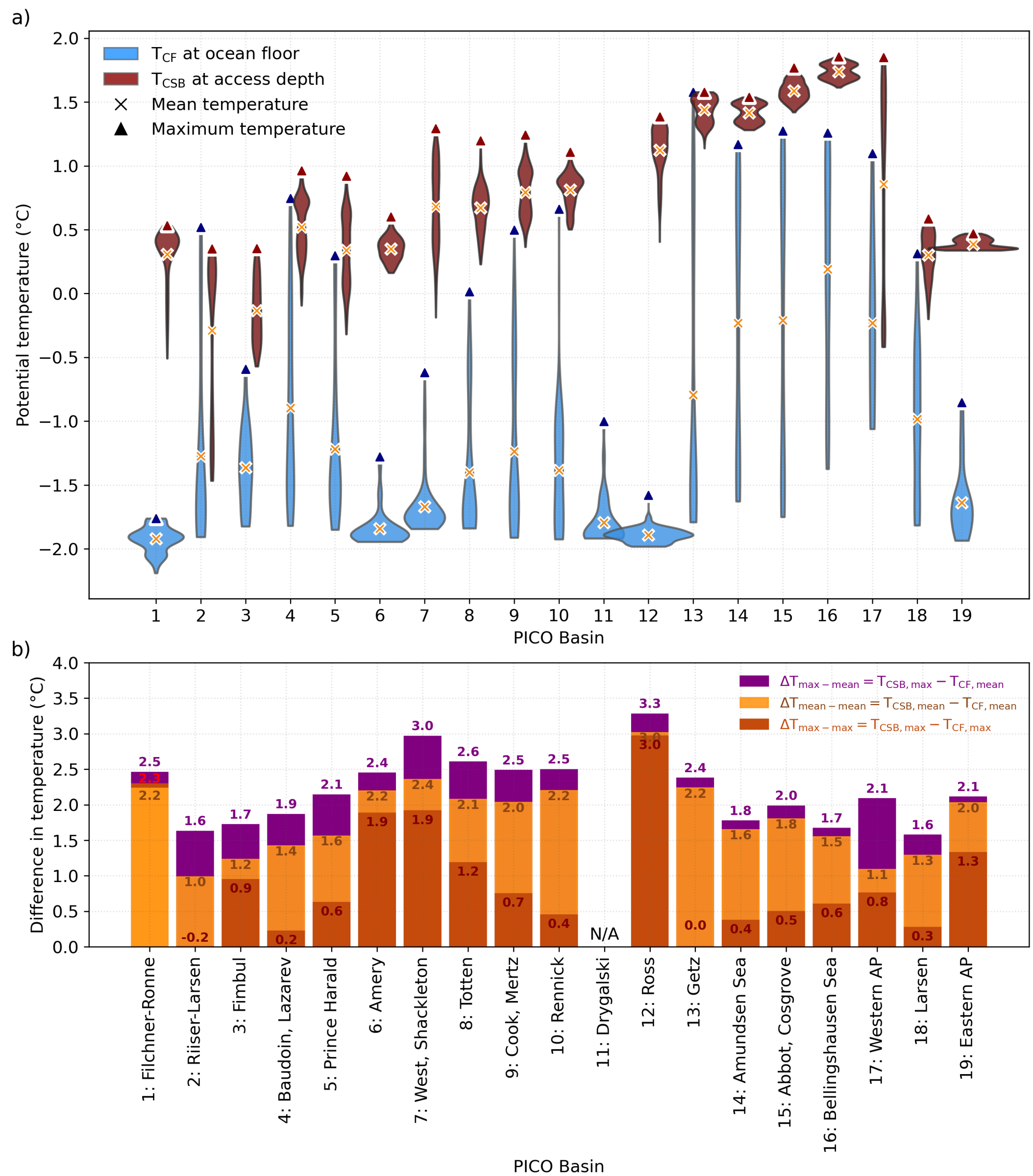

Figure 5. Assessment of extracted temperatures. **a)** The distribution of the T_{CF} (blue) and T_{CSB} (red) estimates for all 19 PICO regions are shown as kernel density estimates, along with the mean and maximum temperatures. The width of the curves depict the approximate frequency of data points within the respective temperature range. T_{CF} incorporates the bottom most temperatures along the calving front, while T_{CSB} is evaluated at the relevant access depth (the deepest along the region's grounding line) at the continental-shelf break, a roughly 40 km wide area where the continental shelf transitions to the open ocean (at 1800 m). Corresponding salinity estimates are found in Supplement Figure S4. **b)** Differences in temperatures from a) when subtracting the mean T_{CSB} ($\Delta T_{\text{mean-mean}}$, orange) and maximum T_{CSB} values from T_{CF} ($\Delta T_{\text{max-max}}$, darkred and $\Delta T_{\text{max-mean}}$, purple), respectively. Temperatures relative to the in situ freezing point, i.e. the thermal driving, is provided in Supplement Fig. S5. Resulting temperature forcing for estimating basin-wide mode 2-melting onset is obtained by adding the differences in b) onto the tuned forcing fields from Reese et al. (2023), see Supplement Fig. S6.

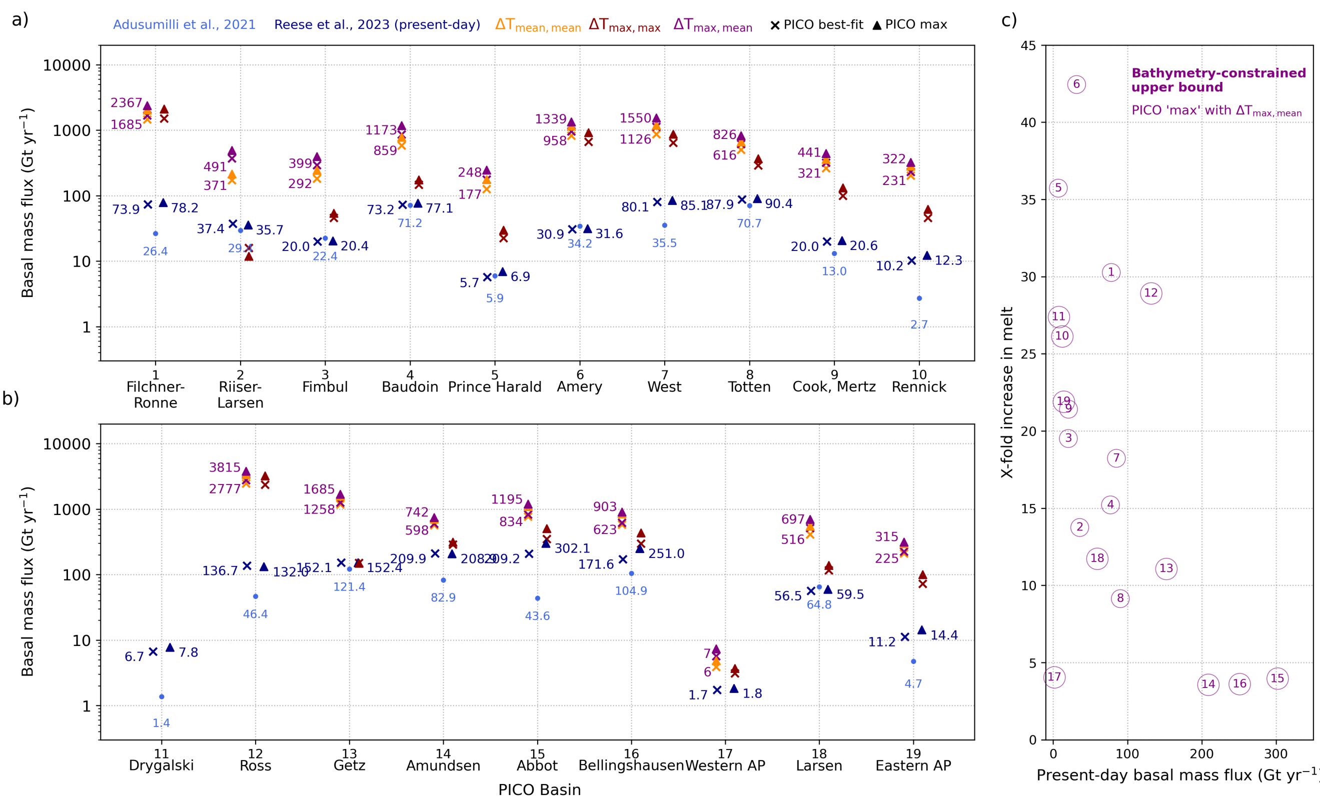

Figure 6. Circum-Antarctic PICO basal mass flux estimates. Estimates for basins 1 to 10 **(a)** and basins 11 to 19 **(b)** when assuming an inflow of warm water masses from the continental-shelf break (orange: comparing mean temperatures, darkred: comparing maximum temperatures, purple: comparing $T_{\mathrm{CSB,\,max}}$ and $T_{\mathrm{CF,\,mean}}$) to present-day basal mass flux estimates of Adusumilli et al. (2020) (lightblue) and the tuned forcing fields of Reese et al. (2023) (darkblue) for two different PICO parameter combination (best-fit and max), respectively. Basin averaged melt rates given in $\mathrm{m\,yr^{-1}}$ are included in Supplement Fig. S7. **c)**: Upper-bound estimates using the 'max' PICO parameter combination relative to present-day basal mass flux from Reese et al. (2023) . The circle-markers indicate the repective basin number.

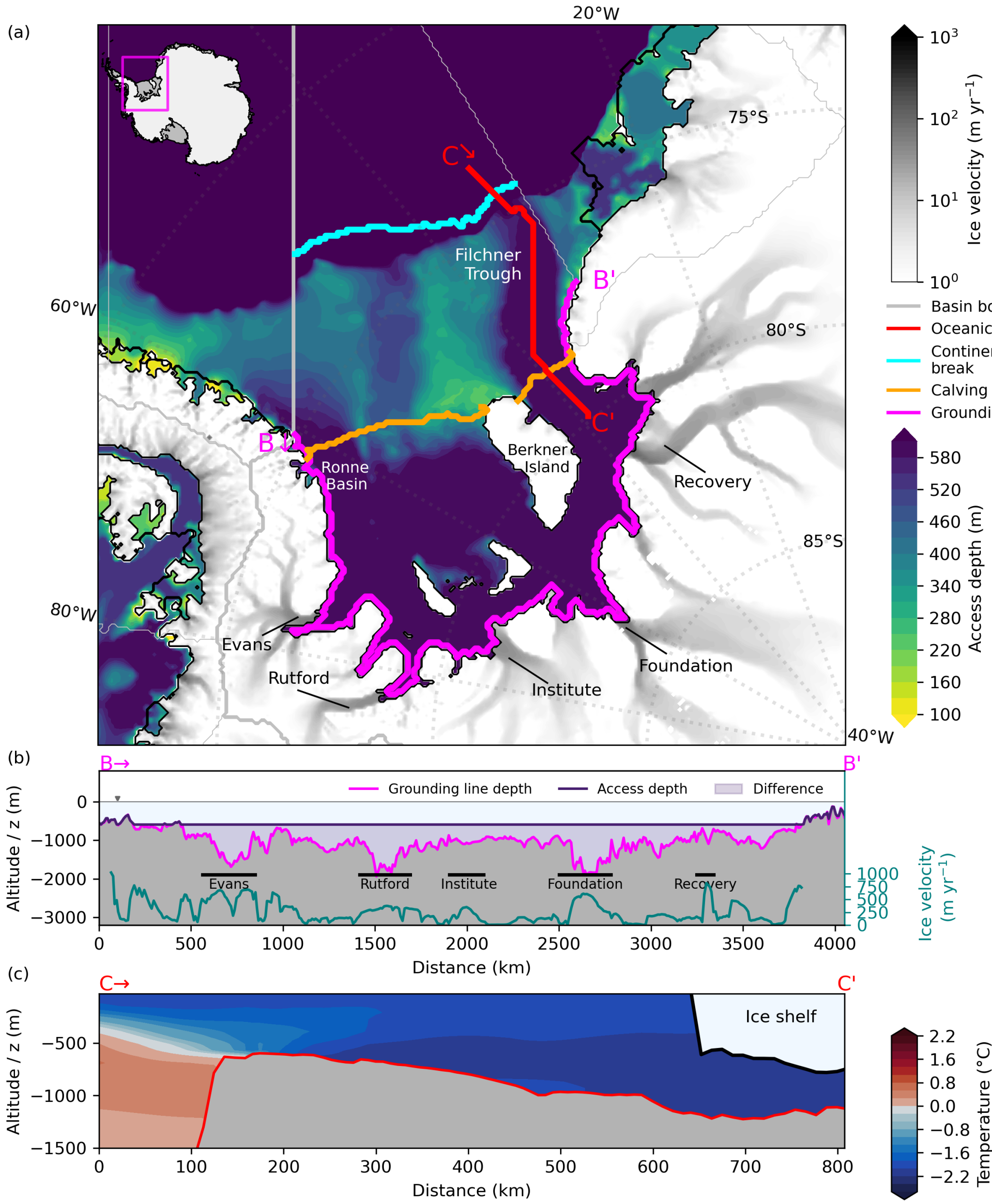

Figure 7. Access depths at Filchner–Ronne Ice Shelf. (a) Access depths within the Weddell Sea indicate a prominent oceanic gateway along Filchner Trough towards Filchner–Ronne Ice Shelf. The transects denote vertical profiles along **(b)** the grounding line and **(c)** the oceanic gateway through Filchner Trough. Speed of grounded ice in grey shading showing the location of major ice streams (in a) and as blue-green line (in b), taken from Mouginot et al. (2019). Magenta line (in b) indicates grounding line depth, while the dark purple line (in b) shows the derived access depth (e.g. $d_{GL,0} = 595$ m throughout most of the cavity).

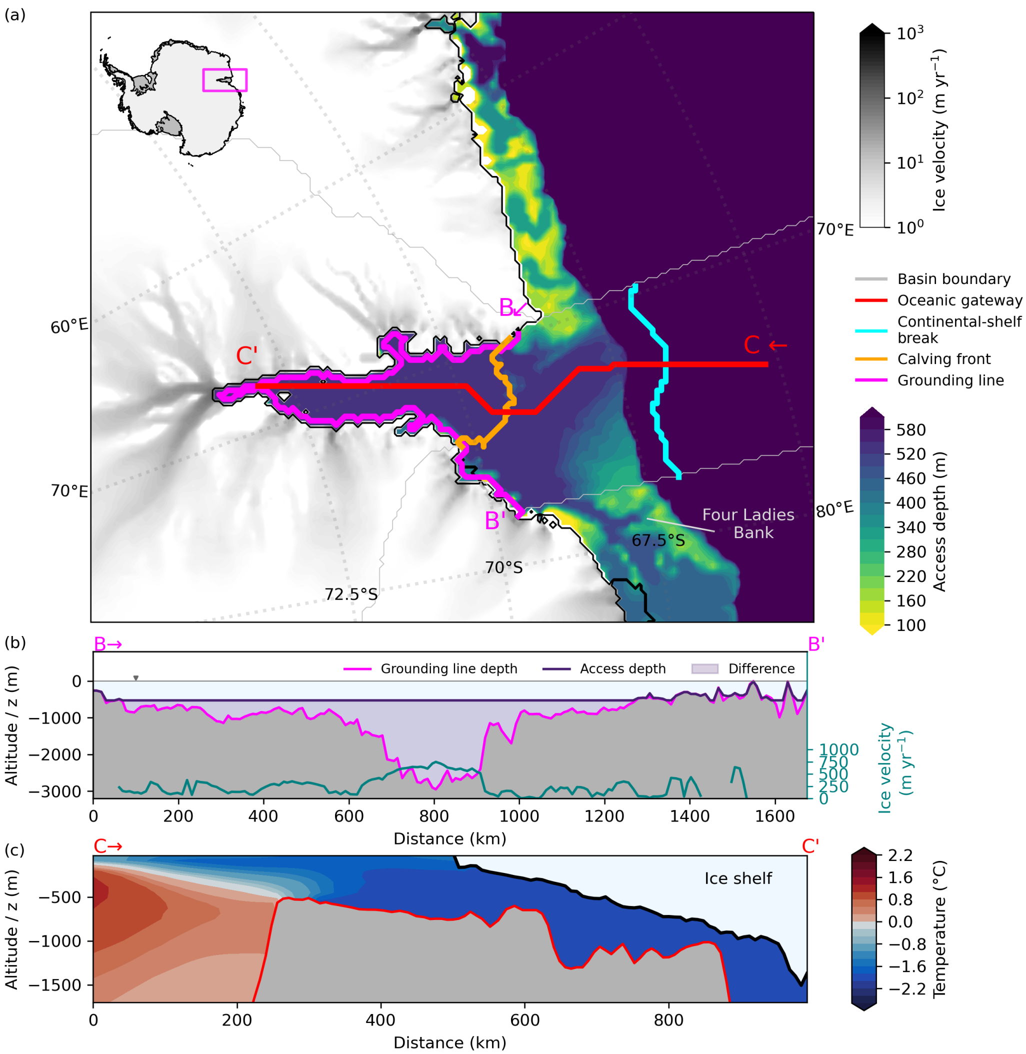

Figure 8. Access depths and temperature profile for Amery Ice Shelf. (a) Computed access depths at Amery Ice Shelf indicate a prominent oceanic gateway along Prydz Channel. The transects denote vertical profiles along **(b)** the grounding line and **(c)** the oceanic gateway through Prydz Channel. Speed of grounded ice in grey shading shows the location of major ice streams (in a) and as blue-green line (in b), taken from Mouginot et al. (2019). Magenta line (in b) indicates grounding line depth, while the dark purple line shows the derived access depth (e.g. $\mathrm{d_{GL,0}} = 525\ \mathrm{m}$ throughout most of the cavity).

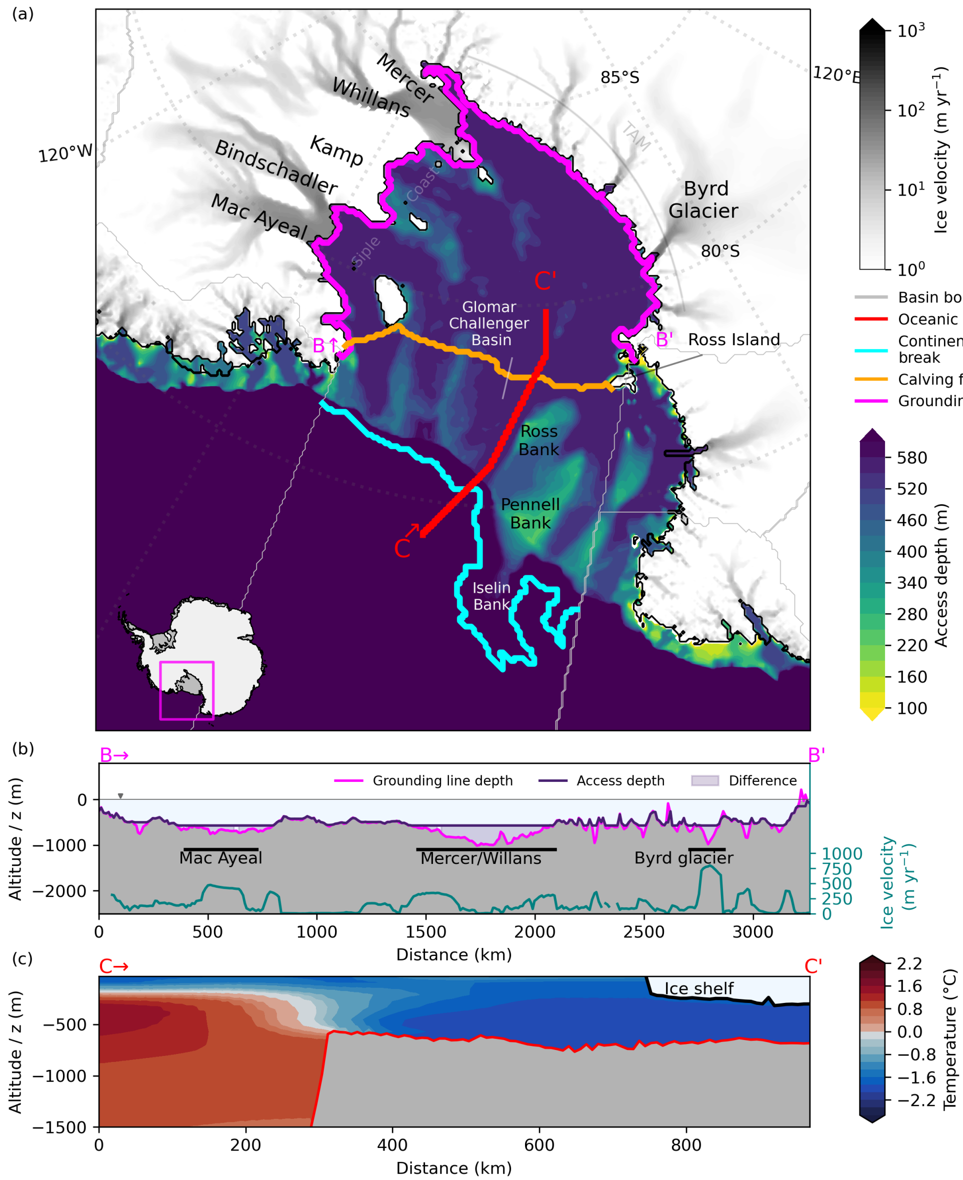

Figure 9. Access depths and temperature profile for Ross Ice Shelf. (a) Computed access depths in the Ross Sea indicate a prominent oceanic gateway through Glomar Challenger Basin towards Ross Ice Shelf. The transects denote vertical profiles along **(b)** the grounding line and**(c)** the oceanic gateway through Glomar Challenger Basin. Speed of grounded ice in grey shading shows the location of major ice streams (in a) and as blue-green line (in b), taken from Mouginot et al. (2019). Magenta line (in b) indicates grounding line depth, while the dark purple line shows the derived access depth. TAM = Transantarctic Mountains.

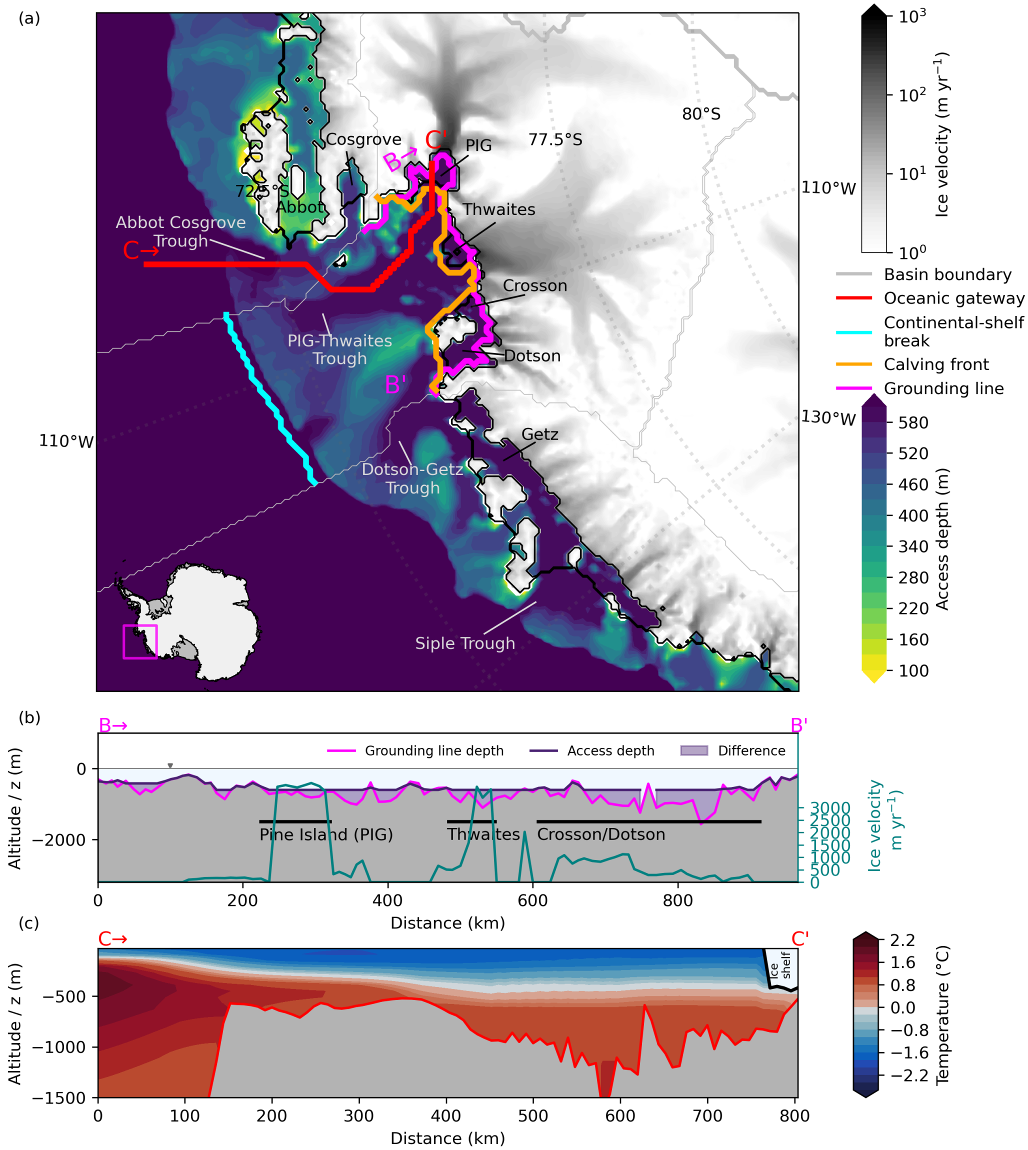

Figure 10. Access depths and temperature profile in the Amundsen Sea region. (a) Computed access depths in the Amundsen Sea indicate a prominent oceanic gateway through Abbot Cosgrove Trough towards Pine Island and Thwaites glaciers. The transects denote vertical profiles along **(b)** the grounding line and **(c)** the pathways from the open ocean to the floating extentsion of Pine Island Glacier. Speed of grounded ice in grey shading showing the location of major ice streams (in a) and as blue-green line (in b), taken from Mouginot et al. (2019). Magenta line (in b) indicates grounding line depth, while the dark purple line (in b) shows the derived access depth (e.g. $d_{GL,0} = 575$ m).

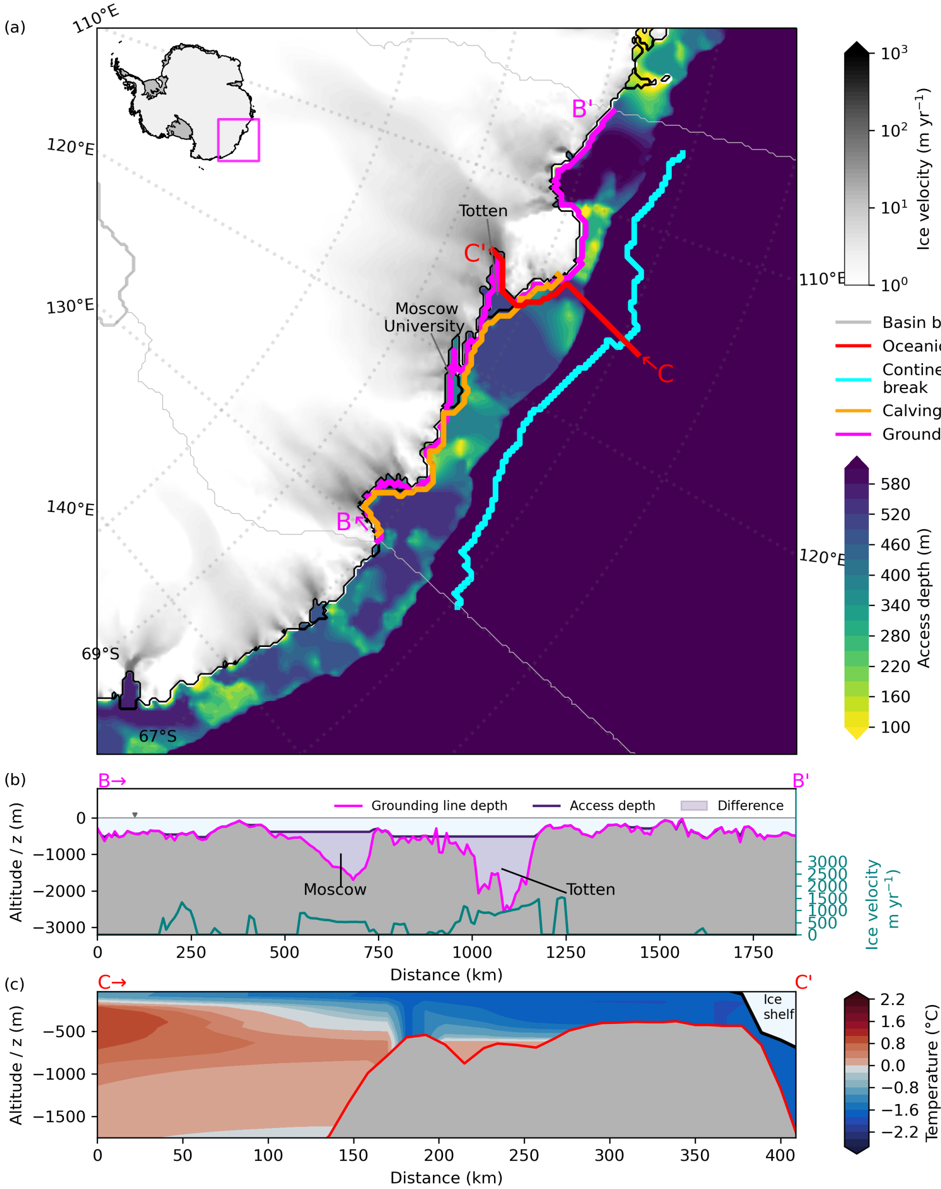

Figure 11. Access depths and temperature profile in the Totten region, East Antarctica. (a) Computed access depths near Totten glacier indicate a prominent oceanic gateway near the Law Dome peninsula (cf. transect C). The transects denote vertical profiles along **(b)** the grounding line and **(c)** the found oceanic gateway. Speed of grounded ice in grey shading showing the location of major ice streams (in a) and as blue-green line (in b), taken from Mouginot et al. (2019). Magenta line (in b) indicates grounding line depth, while the dark purple line (in b) shows the derived access depth at Totten Glacier.

Author contributions. RW conceived the study and together with LN and RR designed the project. LN and RR performed initial analyses and proof of concept. LN made further analyses and together with MK, TA and RR refined the methodology. MK and TA performed the melt experiments. LN made the figures and, together with RR and RW drafted the manuscript, with strong support from all authors.

Competing interests. The authors declare that they have no conflict of interest.

Acknowledgements. LN was financially supported by a stipend from the Studienstiftung des Deutschen Volkes (German National Academic Foundation). LN, RR, MK and RW gratefully acknowledge support by the European Union's Horizon 2020 research and innovation programme under Grant Agreement No. 820575 (TiPACCs). RW further acknowledges support by the European Union's Horizon 2020 under Grant Agreement No. 869304 (PROTECT), by Deutsche Forschungsgemeinschaft (DFG) through grants WI4556/3-1 and WI4556/5-1. MK was financially supported by Deutsche Forschungsgemeinschaft (DFG) through grant WI4556/4-1 and the Potsdam Graduate School. TA and RW acknowledge funding by the PalMod project (FKZ: 01LP1925D, 01LP2305B), supported by the German Federal Ministry of Education and Research (BMBF) as a Research for Sustainability initiative (FONA). RR was supported by the Natural Environment Research Council (NERC) [grant number NE/Y001451/1 RASP]. This work used resources of the Deutsches Klimarechenzentrum (DKRZ) granted by its Scientific Steering Committee (WLA) under project ID bk0993 (PalMod project). The authors gratefully acknowledge the European Regional Development Fund (ERDF), the German Federal Ministry of Education and Research and the Land Brandenburg for supporting this project by providing resources on the high performance computer system at the Potsdam Institute for Climate Impact Research. Development of PISM is supported by NASA grants 20-CRYO2020-0052 and 80NSSC22K0274 and NSF grant OAC-2118285. The authors thank Ralph Timmermann and Hartmut Hellmer for fruitful discussions at an early stage of the project.

References

Adusumilli, S., Fricker, H. A., Medley, B., Padman, L., and Siegfried, M. R.: Interannual variations in meltwater input to the Southern Ocean from Antarctic ice shelves, Nature Geoscience, 13, 616–620, https://doi.org/10.1038/s41561-020-0616-z, 2020.

Alley, R. B., Anandakrishnan, S., Christianson, K., Horgan, H. J., Muto, A., Parizek, B. R., Pollard, D., and Walker, R. T.: Oceanic forcing of ice-sheet retreat: West Antarctica and more, Annual Review of Earth and Planetary Sciences, 43, 207–231, https://doi.org/10.1146/annurev-earth-060614-105344, 2015.

Arndt, J. E., Schenke, H. W., Jakobsson, M., Nitsche, F. O., Buys, G., Goleby, B., Rebesco, M., Bohoyo, F., Hong, J., Black, J., Greku, R., Udintsev, G., Barrios, F., Reynoso-Peralta, W., Taisei, M., and Wigley, R.: The International Bathymetric Chart of the Southern Ocean (IBCSO) Version 1.0—A new bathymetric compilation covering circum-Antarctic waters, Geophysical Research Letters, 40, 3111–3117, https://doi.org/10.1002/grl.50413, 2013.

Asay-Davis, X., Bot, S., and Jourdain, N. C.: ismip/ismip6-antarctic-ocean-forcing: v1.0, https://doi.org/10.5281/zenodo.3997257, 2020.

Assmann, K., Jenkins, A., Shoosmith, D., Walker, D., Jacobs, S., and Nicholls, K.: Variability of Circumpolar Deep Water transport onto the Amundsen Sea continental shelf through a shelf break trough, Journal of Geophysical Research: Oceans, 118, 6603–6620, https://doi.org/10.1002/2013JC008871, 2013.

Bart, P. J.: West-directed flow of the West Antarctic Ice Sheet across eastern basin, Ross Sea during the Quaternary, Earth and Planetary Science Letters, 228, 425–438, https://doi.org/10.1016/j.epsl.2004.10.014, 2004.

Bueler, E. and Brown, J.: Shallow shelf approximation as a “sliding law” in a thermomechanically coupled ice sheet model, Journal of Geophysical Research: Earth Surface, 114, https://doi.org/10.1029/2008JF001179, 2009.

Burgard, C., Jourdain, N. C., Reese, R., Jenkins, A., and Mathiot, P.: An assessment of basal melt parameterisations for Antarctic ice shelves, The Cryosphere, 16, 4931–4975, https://doi.org/10.5194/tc-16-4931-2022, 2022.

Daae, K., Hattermann, T., Darelius, E., Mueller, R. D., Naughten, K. A., Timmermann, R., and Hellmer, H. H.: Necessary conditions for warm inflow toward the Filchner Ice Shelf, Weddell Sea, Geophysical Research Letters, 47, e2020GL089 237, https://doi.org/10.1029/2020GL089237, 2020.

Darelius, E., Daae, K., Dundas, V., Fer, I., Hellmer, H. H., Janout, M., Nicholls, K. W., Sallée, J.-b., and Østerhus, S.: Observational evidence for on-shelf heat transport driven by dense water export in the Weddell Sea, Nature Communications, https://doi.org/10.1038/s41467-023-36580-3, 2023.

De Rydt, J., Holland, P. R., Dutrieux, P., and Jenkins, A.: Geometric and oceanographic controls on melting beneath Pine Island Glacier, Journal of Geophysical Research: Oceans, 119, 2420–2438, https://doi.org/10.1002/2013JC009513, 2014.

Dorschel, B., Hehemann, L., Viquerat, S., Warnke, F., Dreutter, S., Tenberge, Y. S., Accettella, D., An, L., Barrios, F., Bazhenova, E., et al.: The international bathymetric chart of the southern ocean version 2, Scientific Data, 9, 275, https://doi.org/10.1038/s41597-022-01366-7, 2022.

Drijfhout, S. S., Marshall, D. P., and Dijkstra, H. A.: Conceptual models of the wind-driven and thermohaline circulation, in: International Geophysics, vol. 103, pp. 257–282, Elsevier, https://doi.org/10.1016/B978-0-12-391851-2.00011-8, 2013.

Dutrieux, P., De Rydt, J., Jenkins, A., Holland, P. R., Ha, H. K., Lee, S. H., Steig, E. J., Ding, Q., Abrahamsen, E. P., and Schröder, M.: Strong sensitivity of Pine Island ice-shelf melting to climatic variability, Science, 343, 174–178, https://doi.org/10.1126/science.1244341, 2014.

Eisermann, H., Eagles, G., Ruppel, A., Smith, E. C., and Jokat, W.: Bathymetry Beneath Ice Shelves of Western Dronning Maud Land, East Antarctica, and Implications on Ice Shelf Stability, Geophysical Research Letters, 47, e2019GL086 724, https://doi.org/10.1029/2019GL086724, e2019GL086724 2019GL086724, 2020.

Favier, L., Jourdain, N. C., Jenkins, A., Merino, N., Durand, G., Gagliardini, O., Gillet-Chaulet, F., and Mathiot, P.: Assessment of sub-shelf melting parameterisations using the ocean–ice-sheet coupled model NEMO (v3. 6)–Elmer/Ice (v8. 3), Geoscientific Model Development, 12, 2255–2283, https://doi.org/10.5194/gmd-12-2255-2019, 2019.

Flament, T. and Rémy, F.: Dynamic thinning of Antarctic glaciers from along-track repeat radar altimetry, Journal of Glaciology, 58, 830–840, https://doi.org/10.3189/2012JoG11J118, 2012.

Fricker, H. A., Warner, R. C., and Allison, I.: Mass balance of the Lambert Glacier–Amery Ice Shelf system, East Antarctica: a comparison of computed balance fluxes and measured fluxes, Journal of Glaciology, 46, 561–570, https://doi.org/10.3189/172756500781832765, 2000.

Goldberg, D. N., Gourmelen, N., Kimura, S., Millan, R., and Snow, K.: How Accurately Should We Model Ice Shelf Melt Rates?, Geophysical Research Letters, 46, 189–199, https://doi.org/10.1029/2018GL080383, 2019.

Gómez-Valdivia, F., Holland, P. R., Siahaan, A., Dutrieux, P., and Young, E.: Projected West Antarctic ocean warming caused by an expansion of the Ross Gyre, Geophysical Research Letters, 50, e2023GL102 978, https://doi.org/10.1029/2023GL102978, 2023.

Greenbaum, J., Blankenship, D., Young, D., Richter, T., Roberts, J., Aitken, A., Legresy, B., Schroeder, D., Warner, R., Van Ommen, T., et al.: Ocean access to a cavity beneath Totten Glacier in East Antarctica, Nature Geoscience, 8, 294, https://doi.org/10.1038/ngeo238, 2015.

Greene, C. A., Gardner, A. S., Schlegel, N.-J., and Fraser, A. D.: Antarctic calving loss rivals ice-shelf thinning, Nature, 609, 948–953, https://doi.org/10.1038/s41586-022-05037-w, 2022.

Gudmundsson, G. H., Paolo, F. S., Adusumilli, S., and Fricker, H. A.: Instantaneous Antarctic ice sheet mass loss driven by thinning ice shelves, Geophysical Research Letters, 46, 13 903–13 909, https://doi.org/10.1029/2019GL085027, 2019.

Haid, V., Timmermann, R., Gürses, Ö., and Hellmer, H. H.: On the drivers of regime shifts in the Antarctic marginal seas, EGUsphere, pp. 1–18, https://doi.org/10.5194/egusphere-2022-1044, 2022.

Haigh, M., Holland, P. R., and Jenkins, A.: The influence of bathymetry over heat transport onto the Amundsen Sea continental shelf, Journal of Geophysical Research: Oceans, p. e2022JC019460, https://doi.org/10.1029/2022JC019460, 2023.

Hattermann, T.: Antarctic thermocline dynamics along a narrow shelf with easterly winds, Journal of Physical Oceanography, 48, 2419–2443, https://doi.org/10.1175/JPO-D-18-0064.1, 2018.

He, L., Chao, Y., and Suzuki, K.: A run-based one-and-a-half-scan connected-component labeling algorithm, International Journal of Pattern Recognition and Artificial Intelligence, 24, 557–579, https://doi.org/10.1142/s0218001410008032, 2010.

Hein, A. S., Fogwill, C. J., Sugden, D. E., and Xu, S.: Glacial/interglacial ice-stream stability in the Weddell Sea embayment, Antarctica, Earth and Planetary Science Letters, 307, 211–221, https://doi.org/10.1016/j.epsl.2011.04.037, 2011.

Hellmer, H. H., Kauker, F., Timmermann, R., Determann, J., and Rae, J.: Twenty-first-century warming of a large Antarctic ice-shelf cavity by a redirected coastal current, Nature, 485, 225, https://doi.org/10.1038/nature11064, 2012.

Hellmer, H. H., Kauker, F., Timmermann, R., and Hattermann, T.: The Fate of the Southern Weddell Sea Continental Shelf in a Warming Climate, Journal of Climate, 30, 4337–4350, https://doi.org/10.1175/JCLI-D-16-0420.1, 2017.

Herraiz-Borreguero, L., Coleman, R., Allison, I., Rintoul, S. R., Craven, M., and Williams, G. D.: Circulation of modified Circumpolar D eep W ater and basal melt beneath the Amery Ice Shelf, East Antarctica, Journal of Geophysical Research: Oceans, 120, 3098–3112, https://doi.org/10.1002/2015JC010697, 2015.

Heywood, K. J., Schmidtko, S., Heuzé, C., Kaiser, J., Jickells, T. D., Queste, B. Y., Stevens, D. P., Wadley, M., Thompson, A. F., Fielding, S., et al.: Ocean processes at the Antarctic continental slope, Philosophical Transactions of the Royal Society A: Mathematical, Physical and Engineering Sciences, 372, 20130 047, https://doi.org/10.1098/rsta.2013.0047, 2014.

Hirano, D., Tamura, T., Kusahara, K., Fujii, M., Yamazaki, K., Nakayama, Y., Ono, K., Itaki, T., Aoyama, Y., Simizu, D., et al.: On-shelf circulation of warm water toward the Totten Ice Shelf in East Antarctica, Nature Communications, 14, 4955, https://doi.org/10.1038/s41467-023-39764-z, 2023.

Hochmuth, K. and Gohl, K.: Glaciomarine sedimentation dynamics of the Abbot glacial trough of the Amundsen Sea Embayment shelf, West Antarctica, Geological Society, London, Special Publications, 381, 233–244, https://doi.org/10.1144/SP381.21, 2013.

Holland, D. M., Nicholls, K. W., and Basinski, A.: The Southern Ocean and its interaction with the Antarctic Ice Sheet, Science, 367, 1326–1330, https://doi.org/10.1126/science.aaz5491, 2020.

Holland, P. R., O'Connor, G. K., Bracegirdle, T. J., Dutrieux, P., Naughten, K. A., Steig, E. J., Schneider, D. P., Jenkins, A., and Smith, J. A.: Anthropogenic and internal drivers of wind changes over the Amundsen Sea, West Antarctica, during the 20th and 21st centuries, The Cryosphere, 16, 5085–5105, https://doi.org/10.5194/tc-16-5085-2022, 2022.

Jacobs, S., Helmer, H., Doake, C., Jenkins, A., and Frolich, R.: Melting of ice shelves and the mass balance of Antarctica, Journal of Glaciology, 38, 375–387, https://doi.org/10.3189/S0022143000002252, 1992.

Janout, M. A., Hellmer, H. H., Hattermann, T., Huhn, O., Sültenfuss, J., Østerhus, S., Stulic, L., Ryan, S., Schröder, M., and Kanzow, T.: FRIS revisited in 2018: On the circulation and water masses at the Filchner and Ronne Ice Shelves in the southern Weddell Sea, Journal of Geophysical Research: Oceans, 126, e2021JC017 269, https://doi.org/10.1029/2021JC017269, 2021.

Jenkins, A., Dutrieux, P., Jacobs, S., Steig, E. J., Gudmundsson, G. H., Smith, J., and Heywood, K. J.: Decadal ocean forcing and Antarctic ice sheet response: Lessons from the Amundsen Sea, Oceanography, 29, 106–117, https://www.jstor.org/stable/24862286, 2016.

Jenkins, A., Shoosmith, D., Dutrieux, P., Jacobs, S., Kim, T. W., Lee, S. H., Ha, H. K., and Stammerjohn, S.: West Antarctic Ice Sheet retreat in the Amundsen Sea driven by decadal oceanic variability, Nature Geoscience, 11, 733–738, https://doi.org/10.1038/s41561-018-0207-4, 2018.

Jin, J., Payne, A. J., and Bull, C. Y. S.: Current reversal leads to regime change in Amery Ice Shelf cavity in the twenty-first century, EGUsphere, 2024, 1–26, https://doi.org/10.5194/egusphere-2024-1287, 2024.

Jordan, J. R., Miles, B., Gudmundsson, G., Jamieson, S., Jenkins, A., and Stokes, C.: Increased warm water intrusions could cause mass loss in East Antarctica during the next 200 years, Nature Communications, 14, 1825, https://doi.org/10.1038/s41467-023-37553-2, 2023.

Joughin, I., Alley, R. B., and Holland, D. M.: Ice-sheet response to oceanic forcing, Science, 338, 1172–1176, https://doi.org/10.1126/science.1226481, 2012.

Joughin, I., Shapero, D., Dutrieux, P., and Smith, B.: Ocean-induced melt volume directly paces ice loss from Pine Island Glacier, Science advances, 7, eabi5738, https://doi.org/10.1126/sciadv.abi5738, 2021.

Jourdain, N. C., Asay-Davis, X., Hattermann, T., Straneo, F., Seroussi, H., Little, C. M., and Nowicki, S.: A protocol for calculating basal melt rates in the ISMIP6 Antarctic ice sheet projections, The Cryosphere, https://doi.org/10.5194/tc-14-3111-2020, 2020.

Khrulev, C.: PISM's connected component labeling implementation, https://github.com/pism/label-components/, 2024.

Klages, J. P., Kuhn, G., Graham, A. G., Hillenbrand, C.-D., Smith, J., Nitsche, F. O., Larter, R. D., and Gohl, K.: Palaeo-ice stream pathways and retreat style in the easternmost Amundsen Sea Embayment, West Antarctica, revealed by combined multibeam bathymetric and seismic data, Geomorphology, 245, 207–222, https://doi.org/10.1016/j.geomorph.2015.05.020, 2015.

Kreuzer, M., Albrecht, T., Nicola, L., Reese, R., and Winkelmann, R.: Oceanic gateways in Antarctica – Impact of relative sea-level change on sub-shelf melt, EGUsphere, 2023, 1–26, https://doi.org/10.5194/egusphere-2023-2737, 2023.

Lambert, E., Jüling, A., van de Wal, R. S. W., and Holland, P. R.: Modelling Antarctic ice shelf basal melt patterns using the one-layer Antarctic model for dynamical downscaling of ice–ocean exchanges (LADDIE v1.0), The Cryosphere, 17, 3203–3228, https://doi.org/10.5194/tc-17-3203-2023, 2023.

Larter, R. D., Graham, A. G., Hillenbrand, C.-D., Smith, J. A., and Gales, J. A.: Late Quaternary grounded ice extent in the Filchner Trough, Weddell Sea, Antarctica: new marine geophysical evidence, Quaternary Science Reviews, 53, 111–122, https://doi.org/10.1016/j.quascirev.2012.08.006, 2012.

Lewis, E. L. and Perkin, R. G.: Ice pumps and their rates, Journal of Geophysical Research: Oceans, 91, 11 756–11 762, https://doi.org/10.1029/JC091iC10p11756, 1986.

Li, T., Dawson, G. J., Chuter, S. J., and Bamber, J. L.: Grounding line retreat and tide-modulated ocean channels at Moscow University and Totten Glacier ice shelves, East Antarctica, The Cryosphere, 17, 1003–1022, https://doi.org/10.5194/tc-17-1003-2023, 2023.

Mackintosh, A. N., Verleyen, E., O'Brien, P. E., White, D. A., Jones, R. S., McKay, R., Dunbar, R., Gore, D. B., Fink, D., Post, A. L., et al.: Retreat history of the East Antarctic Ice Sheet since the last glacial maximum, Quaternary Science Reviews, 100, 10–30, https://doi.org/10.1016/j.quascirev.2013.07.024, 2014.

Millan, R., Rignot, E., Bernier, V., Morlighem, M., and Dutrieux, P.: Bathymetry of the Amundsen Sea Embayment sector of West Antarctica from Operation IceBridge gravity and other data, Geophysical Research Letters, 44, 1360–1368, https://doi.org/10.1002/2016GL072071, 2017.

Morlighem, M.: MEaSUREs BedMachine Antarctica, Version 3, https://doi.org/10.5067/FPSU0V1MWUB6, [Dataset], accessed 1 July 2022, 2022.

Morlighem, M., Rignot, E., Binder, T., Blankenship, D., Drews, R., Eagles, G., Eisen, O., Ferraccioli, F., Forsberg, R., Fretwell, P., et al.: Deep glacial troughs and stabilizing ridges unveiled beneath the margins of the Antarctic ice sheet, Nature Geoscience, 13, 132–137, https://doi.org/10.1038/s41561-019-0510-8, 2020.

Mouginot, J., Rignot, E., and Scheuchl, B.: Sustained increase in ice discharge from the Amundsen Sea Embayment, West Antarctica, from 1973 to 2013, Geophysical Research Letters, 41, 1576–1584, https://doi.org/10.1002/2013GL059069, 2014.

Mouginot, J., Rignot, E., and Scheuchl, B.: Continent-wide, interferometric SAR phase, mapping of Antarctic ice velocity, Geophysical Research Letters, 46, 9710–9718, https://doi.org/10.1029/2019GL083826, 2019.

Mueller, R. D., Hattermann, T., Howard, S. L., and Padman, L.: Tidal influences on a future evolution of the Filchner–Ronne Ice Shelf cavity in the Weddell Sea, Antarctica, The Cryosphere, 12, 453–476, https://doi.org/10.5194/tc-12-453-2018, 2018.

Naughten, K. A., De Rydt, J., Rosier, S. H., Jenkins, A., Holland, P. R., and Ridley, J. K.: Two-timescale response of a large Antarctic ice shelf to climate change, Nature Communications, 12, 1991, https://doi.org/10.1038/s41467-021-22259-, 2021.

Naughten, K. A., Holland, P. R., Dutrieux, P., Kimura, S., Bett, D. T., and Jenkins, A.: Simulated Twentieth-Century Ocean Warming in the Amundsen Sea, West Antarctica, Geophysical Research Letters, 49, e2021GL094 566, https://doi.org/10.1029/2021GL094566, 2022.

Naughten, K. A., Holland, P. R., and De Rydt, J.: Unavoidable future increase in West Antarctic ice-shelf melting over the twenty-first century, Nature Climate Change, https://doi.org/10.1038/s41558-023-01818-x, 2023.

Nicholls, K. W., Østerhus, S., Makinson, K., Gammelsrød, T., and Fahrbach, E.: Ice-ocean processes over the continental shelf of the southern Weddell Sea, Antarctica: A review, Reviews of Geophysics, 47, https://doi.org/10.1029/2007RG000250, 2009.

Nitsche, F. O., Jacobs, S. S., Larter, R. D., and Gohl, K.: Bathymetry of the Amundsen Sea continental shelf: Implications for geology, oceanography, and glaciology, Geochemistry, Geophysics, Geosystems, 8, https://doi.org/10.1029/2007GC001694, 2007.

Olbers, D. and Hellmer, H.: A box model of circulation and melting in ice shelf caverns, Ocean Dynamics, 60, 141–153, https://doi.org/10.1007/s10236-009-0252-z, 2010.

Owolana, B.: Evaluating the duration of post-LGM grounding events in the Glomar Challenger Basin paleotrough, Eastern Basin Antarctica, using sediment flux calculations, Louisiana State University and Agricultural & Mechanical College, https://doi.org/10.31390/gradschool_theses.3209, 2011.

Paolo, F. S., Fricker, H. A., and Padman, L.: Volume loss from Antarctic ice shelves is accelerating, Science, 348, 327–331, https://doi.org/10.1126/science.aaa0940, 2015.

Pritchard, H., Ligtenberg, S., Fricker, H., Vaughan, D., Van den Broeke, M., and Padman, L.: Antarctic ice-sheet loss driven by basal melting of ice shelves, Nature, 484, 502, https://doi.org/10.1038/nature10968, 2012.

Pritchard, H. D., Arthern, R. J., Vaughan, D. G., and Edwards, L. A.: Extensive dynamic thinning on the margins of the Greenland and Antarctic ice sheets, Nature, 461, 971–975, https://doi.org/10.1038/nature08471, 2009.

Reese, R., Albrecht, T., Mengel, M., Asay-Davis, X., and Winkelmann, R.: Antarctic sub-shelf melt rates via PICO, The Cryosphere, 12, 1969–1985, https://doi.org/10.5194/tc-12-1969-2018, 2018a.

Reese, R., Gudmundsson, G. H., Levermann, A., and Winkelmann, R.: The far reach of ice-shelf thinning in Antarctica, Nature Climate Change, 8, 53, https://doi.org/10.1038/s41558-017-0020-x, 2018b.

Reese, R., Garbe, J., Hill, E. A., Urruty, B., Naughten, K. A., Gagliardini, O., Durand, G., Gillet-Chaulet, F., Gudmundsson, G. H., Chandler, D., Langebroek, P. M., and Winkelmann, R.: The stability of present-day Antarctic grounding lines – Part 2: Onset of irreversible retreat of Amundsen Sea glaciers under current climate on centennial timescales cannot be excluded, The Cryosphere, 17, 3761–3783, https://doi.org/10.5194/tc-17-3761-2023, 2023.

Ribeiro, N., Herraiz-Borreguero, L., Rintoul, S. R., McMahon, C. R., Hindell, M., Harcourt, R., and Williams, G.: Warm Modified Circumpolar Deep Water Intrusions Drive Ice Shelf Melt and Inhibit Dense Shelf Water Formation in Vincennes Bay, East Antarctica, Journal of Geophysical Research: Oceans, 126, e2020JC016 998, https://doi.org/10.1029/2020JC016998, e2020JC016998 2020JC016998, 2021.

Rignot, E., Jacobs, S., Mouginot, J., and Scheuchl, B.: Ice-shelf melting around Antarctica, Science, 341, 266–270, https://doi.org/10.1126/science.1235798, 2013.

Schmidtko, S., Heywood, K. J., Thompson, A. F., and Aoki, S.: Multidecadal warming of Antarctic waters, Science, 346, 1227–1231, https://doi.org/10.1126/science.1256117, 2014.

Silvano, A., Rintoul, S. R., and Herraiz-Borreguero, L.: Ocean-ice shelf interaction in East Antarctica, Oceanography, 29, 130–143, http://www.jstor.org/stable/24862288, 2016.

Sun, C., Liu, C., Wang, Z., Yan, L., Tao, Y., Qin, Q., and Qian, J.: On the influences of the continental shelf bathymetry correction in Prydz Bay, East Antarctica, Frontiers in Marine Science, 9, 957 414, https://doi.org/10.3389/fmars.2022.957414, 2022.

Thoma, M., Jenkins, A., Holland, D., and Jacobs, S.: Modelling circumpolar deep water intrusions on the Amundsen Sea continental shelf, Antarctica, Geophysical Research Letters, 35, https://doi.org/10.1029/2008GL034939, 2008.

Thompson, A. F., Stewart, A. L., Spence, P., and Heywood, K. J.: The Antarctic Slope Current in a Changing Climate, Reviews of Geophysics, 56, 741–770, https://doi.org/https://doi.org/10.1029/2018RG000624, 2018.

Tinto, K., Padman, L., Siddoway, C., Springer, S., Fricker, H., Das, I., Caratori Tontini, F., Porter, D., Frearson, N., Howard, S., et al.: Ross Ice Shelf response to climate driven by the tectonic imprint on seafloor bathymetry, Nature Geoscience, 12, 441–449, https://doi.org/10.1038/s41561-019-0370-2, 2019.

van der Linden, E. C., Le Bars, D., Lambert, E., and Drijfhout, S.: Antarctic contribution to future sea level from ice shelf basal melt as constrained by ice discharge observations, The Cryosphere, 17, 79–103, https://doi.org/10.5194/tc-17-79-2023, 2023.

Walker, D. P., Brandon, M. A., Jenkins, A., Allen, J. T., Dowdeswell, J. A., and Evans, J.: Oceanic heat transport onto the Amundsen Sea shelf through a submarine glacial trough, Geophysical Research Letters, 34, https://doi.org/10.1029/2006GL028154, 2007.

Wang, Y., Zhou, M., Zhang, Z., and Dinniman, M. S.: Seasonal variations in Circumpolar Deep Water intrusions into the Ross Sea continental shelf, Frontiers in Marine Science, 10, https://doi.org/10.3389/fmars.2023.1020791, 2023.

Williams, G. D., Herraiz-Borreguero, L., Roquet, F., Tamura, T., Ohshima, K. I., Fukamachi, Y., Fraser, A. D., Gao, L., Chen, H., McMahon, C. R., Harcourt, R., and Hindell, M.: The suppression of Antarctic bottom water formation by melting ice shelves in Prydz Bay, Nature Communications, 7, 12 577, https://doi.org/10.1038/ncomms12577, 2016.

Winkelmann, R., Martin, M. A., Haseloff, M., Albrecht, T., Bueler, E., Khroulev, C., and Levermann, A.: The Potsdam parallel ice sheet model (PISM-PIK)–Part 1: Model description, The Cryosphere, 5, 715–726, https://doi.org/10.5194/tc-5-715-2011, 2011.

Zwally, H. J., Giovinetto, M. B., Beckley, M. A., and Saba, J. L.: Antarctic and Greenland Drainage Systems, http://imbie.org/imbie-3/drainage-basins/, [Dataset], accessed 27 November 2018, 2012.